Modeling burial and thermal history of the central European basins and comparison with organic maturity data

Master's thesis
submitted in fulfilment
of the requirements for the degree
Master of Science (M.Sc.)
in Geoscience

January 2017
Georg-August-University Göttingen
Faculty of Geosciences and Geography
Department of Structural Geology and Geodynamics
Geoscience Center

by

Tom Kaltofen

Born in Berlin

Supervisor:	Dr. Elco Luijendijk
Co-supervisor:	Prof. Dr. Jonas Kley

Contents

Abstract

For individual basins, geological events such as exhumation and volcanism are thermally well-understood. However, platforms for comparing thermal histories between individual basins over complex basin systems are scarce, which leads to questions when analyzing timings or extends of large scale thermal events. Therefore, our objective is to quantify subsurface temperature and maturation for the Central European Basin System. We model burial and thermal history of this basin using recently published stratigraphic data and compare our modeled thermal history to basin-wide compilations of present-day subsurface temperature and organic maturity data of the top Carboniferous. Modeled subsurface temperatures are close to published subsurface temperature data. The comparison in organic maturity data shows strong misfit in the Northeast German Basin. We traced the key reasons for the misfit back to Lower Rotliegend volcanic rocks and the Variscan deformation front, but also to the Late Cretaceous inversion. The location of the Variscan deformation front is discussed from the point of view of thermal history. With this analysis, we show that sub-basins are thermally comparable within our model. In addition, the validity of the heavy-tail relationship of the Sadler effect in the Central European Basin System is analyzed and partially confirmed. Links between accumulation rates and deposition regimes are drawn in the Lower Saxony Basin and Glueckstadt Graben.

1 Introduction

The Carboniferous to Permian thermal history of the Central European Basin System (CEBS) [*Ziegler*, 1990] is influenced by volcanism and exhumation, for which the causes and scales are partially unknown [*Meier et al.*, 2016]. Especially, the sub-Permian angular unconformity is marked by a separation in organic maturity as a result of the prograding Variscan deformation front [*Drozdzewski et al.*, 2009].

This separation of organic maturity is partly explainable by heating of large volcanic successions [*Heeremans et al.*, 2004; *Wilson et al.*, 2004], high heat flows [*Resak et al.*, 2008; *Kerschke and Schulz*, 2013] and exhumation, as well as erosion due to the development of the Variscan deformation front, whose extent is in discussion for the German [*Drozdzewski et al.*, 2009; *Dulce and Lewis*, 2011] and Polish part [*Mazur et al.*, 2010; *Krzywiec et al.*, 2016]. In those studies, the volcanic succession and Variscan deformation front were studied via seismic and lithological data, yet not systematically in respect to their thermal histories.

Nevertheless, several individual sedimentary basins underwent research regarding their thermal history, such as the Lower Saxony Basin [*Petmecky et al.*, 1999], the Glueckstadt Graben [*Rodon and Littke*, 2005], the Polish Trough [*Resak et al.*, 2008] and the Roer Valley Graben [*Luijendijk et al.*, 2011a]. Additionally, organic maturity data compilations of the top Carboniferous exist for the area of the CEBS [*Koch et al.*, 1997; *Gerling et al.*, 1999; *Doornenbal and Stevenson*, 2010; *Botor et al.*, 2013].

Furthermore, a crustal model [*Maystrenko and Scheck-Wenderoth*, 2013], as well as considerations about the differences of the tectonic structure [*Scheck-Wenderoth and Lamarche*, 2005], the sedimentary fill [*Van Wees et al.*, 2000] and various salt tectonics [*Maystrenko et al.*, 2013] within the CEBS are published.

Large scale present subsurface temperature models are in research worldwide [*Bertani*, 2016] and in Europe [*Cacace et al.*, 2013; *Scheck-Wenderoth and Maystrenko*, 2013; *Limberger*, 2014; *Scheck-Wenderoth et al.*, 2014]. They deliver subsurface temperature and heat flow model data compilations. Different authors study subsurface temperature model conditions [*Noack et al.*, 2012; *Fuchs et al.*, 2015; *Fuchs and Balling*, 2016b] and compare different subsurface temperature model approaches [*Fuchs and Balling*, 2016a]. However, large subsurface temperature models of the geologic history are not available for the CEBS.

Therefore, we model at large scale the subsurface temperature and organic maturity within the CEBS from the surface up to the bottom of Upper Rotliegend with a thermal burial history model. For calibration, organic maturity and subsurface temperature compilations, as well as borehole data are compared to our model results and used to adjust model parameters. With these organic maturity model results, we aim to describe the separation of the organic maturity around the sub-Permian angular unconformity with arguments from thermal history.

In the chapter of the Sadler effect, we describe its theory and relevance to this study. Furthermore, the hypothesis of the Sadler effect power law is tested in the CEBS and links between accumulation rates and deposition regimes are drawn.

1.1 Paleozoic geological history of the study area

The term CEBS was first described by *Ziegler* [1990], where many authors left their marks in geologic research history [*Littke et al.*, 2008; *Doornenbal and Stevenson*, 2010] (Figure 1). The CEBS developed on top of mixed mosaic crustal domains in ages from Precambrian to Carboniferous [*Van Wees et al.*, 2000]. Important crustal domains in the CEBS are the Variscan crust, the Caledonian crust of Avalonia and Laurentia, as well as the Precambrian crust of Baltica with the East European Craton [*Pharaoh*, 1999].

The structure of the study area is marked by the Trans-European-Suture-Zone, which is split into the northern Sorgenfrei-Tornquist-Zone and southern Teisseyre-Tornquist-Zone. This southern Zone divides the Paleozoic crust of western Europe from Precambrian crust of the East European Craton [*Hossein et al.*, 2006]. The East European Craton is an old and thick crust with low heat flows and thermal ages older than 800 million years [*Hossein et al.*, 2006]. The Paleozoic crust in the west of the Teisseyre-Tornquist-Zone is younger and shows higher heat flows [*Goesl and Govers*, 2000].

For the area of the CEBS, *Hossein et al.* [2006] rework ideas of *Thybo* [2000] into four major tectonic events in the Phanerozoic geological evolution: the Late Cretaceous inversion, the Mesozoic rifting with the formation of graben structures, the Variscan orogeny and the Caledonian collision tectonics. The Caledonian collision tectonics took place from Cambrian up to the Early Devonian [*Doornenbal and Stevenson*, 2010], which is out of scope of this study.

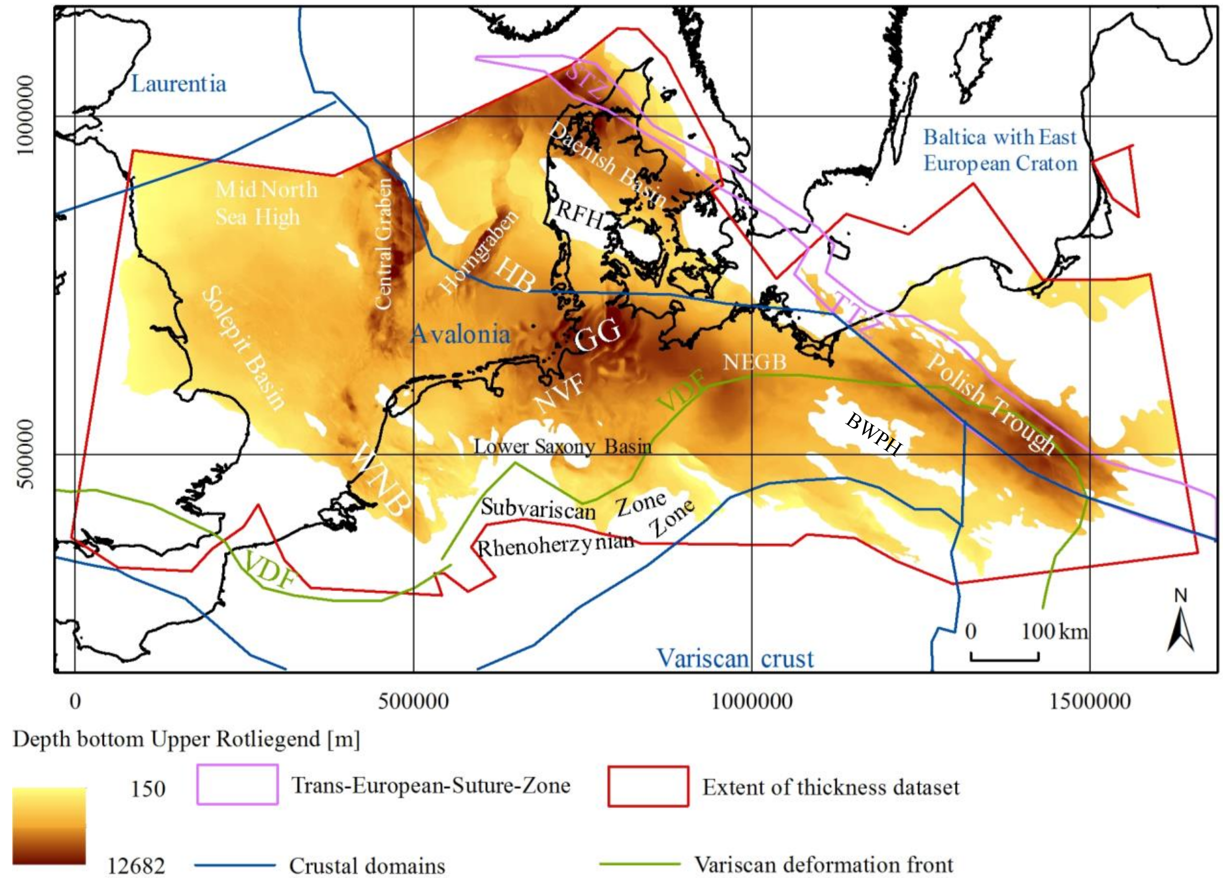

Figure 1. Extent of thickness dataset [*Doornenbal and Stevenson*, 2010] defines extent of study area. Geological features are adapted from *Doornenbal and Stevenson* [2010] and *Drozdzewski et al.* [2009]. West Netherlands Basin (WNB), Helgoland Basin (HB), Glueckstadt Graben (GG), Northeast German Basin (NEGB), Ringkøbing-Fyn high (RFH), Sorgenfrei-Tornquist-Zone (STZ), Teisseyre-Tornquist-Zone (TTZ), North Variscan Foreland (NVF), Brandenburg-Wolsztyn-Pogorzela high (BWPH).

Between Early Devonian and Early Permian, Gondwana collided with Laurussia forming the Variscan orogeny [*Doornenbal and Stevenson*, 2010]. In the Early Carboniferous, southwards subduction beneath mid-European terranes lead to the formation of the Variscan Mountains [*Stampfli et al.*, 2002].

During the following period, the Variscan deformation front migrated northwards [*Kroner and Romer*, 2013]. Close to the orogeny, flexural basin developed, which were later deformed into the Paleozoic thrust and fold complexes of the Rhenohercynian Zone and Subvariscan Zone [*Franke*, 1995]. These Paleozoic zones are separated from wrench induced basins by the Variscan deformation front in a 10 to 20 km wide zone [*Drozdzewski et al.*, 2009].

It is assumed that the Variscan deformation decreases gradually towards the foreland [*Franke*, 1995] and different deformation styles are observed, such as a thrust zone near the Brabant Massif or synclines and anticlines in connection with upthrusting in the Ruhr Basin [*Von Hartmann*, 2003]. Up to 7000 m thick sediments accumulated in the foredeep due to the load of the Variscan orogeny during Namurian (326 -313 Ma) and Westphalian (316.5 – 306 Ma) [*Menning et al.*, 2005], whereas 5000 m thick sediments are observed at the tectonic highs at the northern basin margins [*Drozdzewski et al.*, 2009].

The migration of the deformation front terminated during late Westphalian or Stephanian (306 - 300 Ma) [*Menning et al.*, 2005; *Drozdzewski et al.*, 2009]. The deformation in the Subvariscan Zone resulted in an angular unconformity between Carboniferous formations and Upper Rotliegend [*Drozdzewski et al.*, 2009], in which deep buried Carboniferous formations exhumed and subsequently eroded. However, the mechanisms behind the uplifting are not well constrained [*Drozdzewski et al.*, 2009].

For the area north of the Variscan deformation front (North Variscan Foreland), the amounts of eroded material in the period of the unconformities between Carboniferous and Upper Rotliegend are of less size [*Drozdzewski et al.*, 2009].

Not to be confused with the aforementioned unconformities, the Saalian unconformity divides Lower Rotliegend from Upper Rotliegend, in which a period of non-deposition took place (time gap of 8 to 20 million years) [*Heeremans et al.*, 2004]. Lower Rotliegend rocks are mostly preserved in the North Sea, eastern parts of Germany and northwest of Poland [*Timmerman*, 2004]. The Lower Rotliegend consists of volcanic successions and locally clastics, while Upper Rotliegend is mainly of sedimentary origin [*Heeremans et al.*, 2004]. However, the aforementioned unconformities coincide often with the Saalian unconformity, since Lower Rotliegend is mostly not preserved.

This period is linked to extensive magmatic provinces [*Heeremans et al.*, 2004] and associated extensional tectonics [*Wilson et al.*, 2004] during the Stephanian to early Permian [*Timmerman*, 2004] in the CEBS. *Wilson et al.* [2004] argues that this period is a stress response to the tectonic disintegration of the Variscan orogeny.

Since this period, the subsidence within the CEBS was probably dominated by thermal relaxation and sedimentary loading [*Littke et al.*, 2008]. During the Permian, the subsidence within the study area continued and the depositional environment changed from terrestrial (Upper Rotliegend) to an evaporitic regime with the deposition of salts and carbonates (Zechstein formation) [*Doornenbal and Stevenson*, 2010].

1.2 Mesozoic geological history

The breaking up of Pangaea in Triassic times resulted in the formation of different basins like the Glueckstadt Graben, the Horngraben and the Central Graben [*Yegorova et al.*, 2007]. Salt tectonics lead to decoupling between the footwall of the salt and the subsequent cover [*Yegorova et al.*, 2007]. Several thousand meters of sediments accumulated in local basins, such as in the Glueckstadt Graben (9000 m) or the Horngraben (6000 m) [*Doornenbal and Stevenson*, 2010]. During the subsequent rifting stages in Triassic to Jurassic times, the basins were filled with a mixture of continental and marine deposits in the Triassic and predominantly marine shales and carbonates in the Jurassic [*Littke et al.*, 2008].

Towards the Early Cretaceous, the sea level decreased and the depositional regime of the CEBS changed to more continental conditions [*Littke et al.*, 2008]. In the Late Cretaceous, it is assumed that high global rates of seafloor spreading caused a period of elevated sea level, in which dominantly carbonates accumulated within the CEBS [*Littke et al.*, 2008].

During the Late Cretaceous and early Cenozoic, a compressional regime lead to partial inversion of the CEBS [*Yegorova et al.*, 2007]. *Kley and Voigt* [2008] pinpoint the compressional regime to stresses within the central Europe's lithosphere in response to African-Iberia-Europe convergence.

In the Cenozoic and Quaternary, the proportions of continental sediments increased [*Doornenbal and Stevenson*, 2010]. Overall, thickness differences between lithologies of sub-basins point to strong segmentation of the CEBS [*Maystrenko and Scheck-Wenderoth*, 2013] and altogether, these multi-dimensional geological features define the complexity of this basin system [*Littke et al.*, 2008].

2 Methods

2.1 Burial and thermal history model

We simulate the burial history and thermal history of sediments using the one-dimensional burial history and heat flow model Pybasin [*Luijendijk et al.*, 2011a]. Burial history is calculated from observed present-day thickness of stratigraphic units using standard back stripping methods [*Steckler and Watts*, 1978; *Bond and Kominz,* 1984].

We gridded the study area in 5 km grid cells. For each grid cell, we ran a single one-dimensional burial and thermal history model, resulting in a quasi-four-dimensional burial history model. We excluded salt structures, pillows and diapirs according to the Southern Permian Basin Atlas (SPBA) [*Doornenbal and Stevenson*, 2010], to avoid areas where the true burial history and heat flow is unlikely represented by our one-dimensional model.

Compaction and the resulting change in thickness of sediments is calculated using an exponential porosity-depth equation [*Athy*, 1930; *Luijendijk et al.*, 2011a]:

$$\phi = \phi_0 \, e^{-cz}, \tag{1}$$

with ϕ as porosity. $\phi_0$describes the initial porosity at surface, z is depth (m) and c is compressibility (m^{-1}).

Our thermal history model is based on the burial model and solves a heat conduction equation using the finite difference method [*Courant*, 1943] under the assumption that in sedimentary basins most heat is transferred vertically by conduction [*Scheck-Wenderoth et al.*, 2014]. The used heat conduction equation is based on an implicit numerical finite solution:

$$\rho c \, \frac{\partial T}{\partial t} = \nabla K \nabla T + Q, \tag{2}$$

where T is temperature (°C), t is time (s), K is thermal conductivity (W m^{-1} K^{-1}), Q is heat production (W m^{-3}), c is heat capacity (J kg^{-1} K^{-1}) and ρ is density (kg m^{-3}).

2.2 Input of thermal history model

We used a specified heat flux as lower boundary condition (Figure 2) and a specified temperature as upper boundary condition (Figure 3). For the heat flux of the lower boundary condition, the modeled heat flow data at the base of the Permian Zechstein formation by *Scheck-Wenderoth et al.* [2014] was taken as input. These heat flow data are based on a crustal heat flow model with two thermal boundary conditions, which are along the top surface and along the base of modeled lithosphere-asthenosphere boundary [*Scheck-Wenderoth et al.*, 2014]. The depth of the lithosphere-asthenosphere boundary is based on geophysical data [*Maystrenko and Scheck-Wenderoth*, 2013; *Maystrenko et al.*, 2013; *Scheck-Wenderoth and Maystrenko*, 2013]. The heat flux variability of this input data is around 55 to 77 mWm^{-2}. A part of the study area is not covered by the basal heat flow dataset (Figure 2). For this area, we assume a heat flux of 50 mWm^{-2}.

The surface temperature boundary (Figure 3) is based on reconstructed surface temperature history over the Mesozoic and Cenozoic [*Helsen and Langenaeker*, 1999; *Luijendijk et al.*, 2011a].

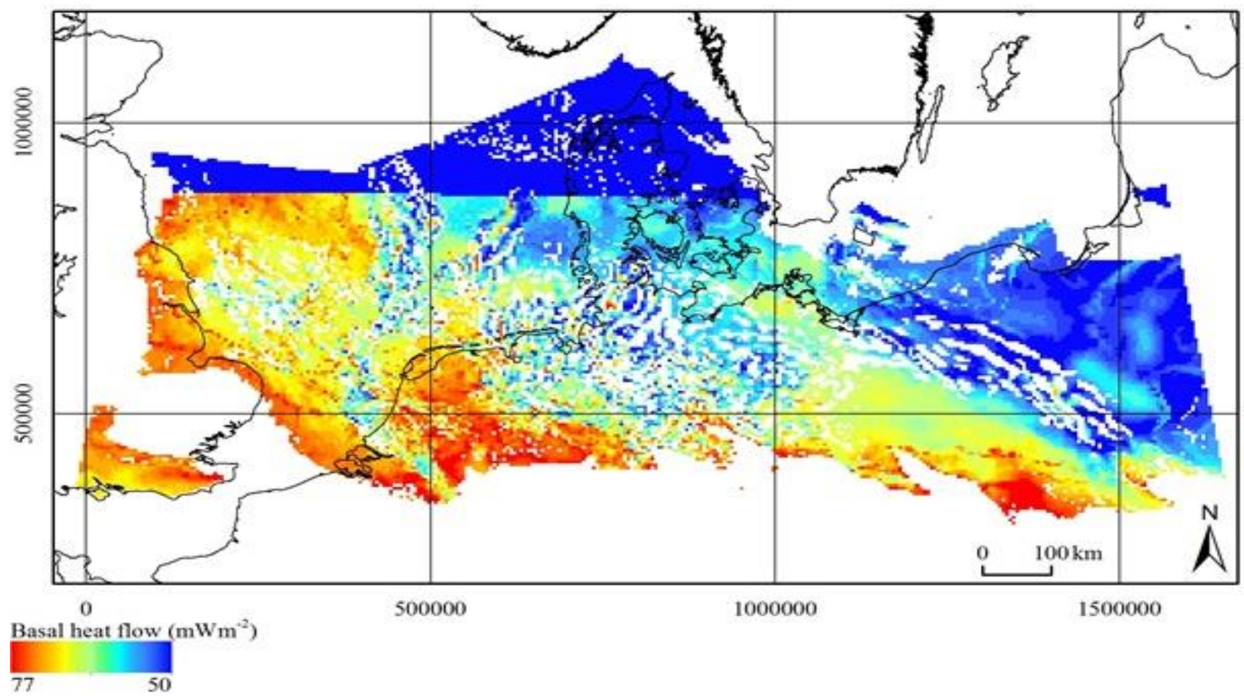

Figure 2. Utilized basal heat flow values as input into the model of this study. The basal heat flow of 50 mWm^{-2} is taken in our model to show the influence of the input basal heat flow onto the modeled temperature, while other values are taken from the base of Zechstein formation modeled by *Scheck-Wenderoth et al.* [2014]

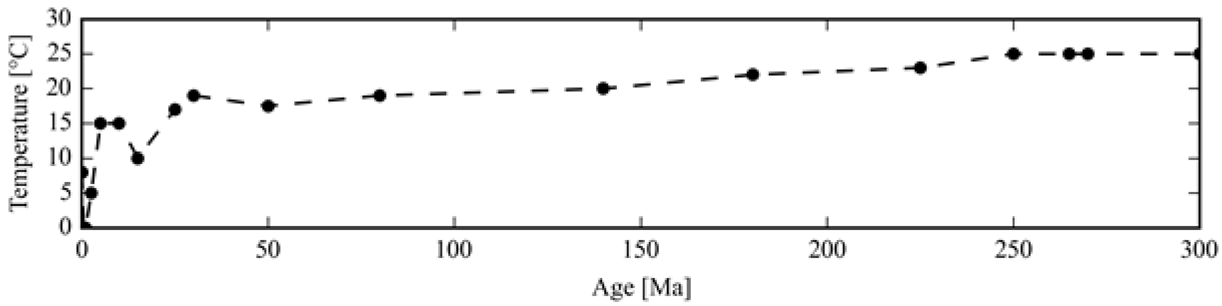

Figure 3. Assumed surface temperatures in this study [*Helsen and Langenaeker*, 1999; *Luijendijk et al.*, 2011a]. Dots are actual input data, while lines are interpolated by Pybasin.

2.3 Lithology

The modeled porosity and thermal conductivity are dependent on lithology. Our lithological input is based on published lithostratigraphic data of the SPBA, which is a compilation of data by industry and geological surveys [*Doornenbal and Stevenson*, 2010]. We adapted the age and lithology definition of this atlas for this study (Table 1). The surface elevation dataset ETOPO1 [*Amante and Eakings*, 2009] was chosen for constraining the top of the Quaternary. We excluded areas with less than 3 lithostratigraphic units or less than 500 m total depth, because modeled subsurface temperatures and organic maturity values unlikely represent true subsurface temperature conditions or are below calculation limit by our model.

Table 1. Age definitions in thickness dataset[1]

Stratigraphic unit	Quaternary	Tertiary	Upper Cretaceous	Lower Cretaceous	Upper Jurassic	Middle Jurassic
Top age (Ma)	0	3	66	100	145	163
Bottom age (Ma)	3	66	100	145	163	175
Stratigraphic unit	Lower Jurassic	Upper Triassic	Middle Triassic	Lower Triassic	Zechstein	Upper Rotliegend
Top age (Ma)	175	201	235	247	252	258
Bottom age (Ma)	201	235	247	252	258	265

[1]Ages according to *Doornenbal and Stevenson* [2010]

The input thermal conductivity parameters of the literature are often given as bulk rock conductivity [*Scheck-Wenderoth et al.*, 2014; *Fuchs and Balling*, 2016b], whereas we specify rock and pore space thermal properties separately into our model.

The model input parameters rock density [*Yegorova et al.*, 2007; *Luijendijk et al.*, 2011a; *Maystrenko and Scheck-Wenderoth*, 2013], surface porosity and compressibility [*Revil and Cathles*, 1999; *Luijendijk et al.*, 2011a; *Schoen*, 2015] were chosen to match recent literature. Heat capacity and heat production are based on *Luijendijk et al.* [2011a].

To approach more realistic values for rock properties, we started to model low subsurface temperature values and then calibrated the rock properties to fit our modeled data to data compilations and borehole data. This low subsurface temperature approach is chosen because our model calculates organic maturity excluding heat sources such as volcanism, fluid flow or exhumation. Thus, our model results of organic maturity should be equal or lower than organic maturity of measured data. Therefore, it makes sense to converge from low organic maturity and hence, low subsurface temperatures. Because high thermal conductivity values lead to low temperatures, high thermal conductivity values were adapted from *Fuchs and Balling* [2016b] as rock thermal properties and modified by considering other literature [*Clauser and Huenges*, 2013; *Schoen*, 2015] as starting point for calibration of model parameters (Table 2).

Table 2. At start used rock properties in our model, which were subject to calibration

Stratigraphic unit	Lithology[1]	Density (Kg m^{-3})	Surface Porosity[6] (%)	Compressibility[6] (m^{-1})	Thermal Conductivity (W $m^{-1}K^{-1}$)	Heat Capacity[5] (J $kg^{-1}K^{-1}$)	Heat Production[5] (W m^{-3})
Quaternary	Sand, Silt and Clay	2100[4]	0.45	3.95E-4	3.4[2]	900	1.25E-6
Tertiary	Sand, Silt and Clay	2300[4]	0.45	3.95E-4	3.4[2]	900	1.25E-6
Upper Cretaceous	Limestone	2390[4]	0.5	7.90E-4	3.7[2]	900	1.25E-6
Lower Cretaceous	Clay with Sand and Silt	2480[3]	0.55	5.00E-4	3.2[2]	900	1.25E-6
Upper Jurassic	Clay with Sand, Silt and Marl	2480[3]	0.5	5.00E-4	3.0[2]	900	1.25E-6
Middle Jurassic	Clay with Sand, Silt and Marl	2480[3]	0.5	5.00E-4	2.1[2]	900	1.25E-6
Lower Jurassic	Clay with Sand, Silt and Marl	2480[3]	0.5	5.00E-4	2.6[2]	900	1.25E-6
Upper Triassic	Clay with Marl and Gypsum	2480[3]	0.55	5.00E-4	2.9[2]	900	1.25E-6
Middle Triassic	Limestone	2480[3]	0.5	7.90E-4	3.1[2]	900	1.25E-6
Lower Triassic	Clastics with Evaporites	2480[3]	0.35	5.00E-4	3.1[2]	900	1.25E-6
Zechstein	Carbonate, Anhydrite and Clastic	2480[3]	0.2	7.90E-7	5.8[2]	900	1.25E-6
Upper Rotliegend	Clay, silt and Sandstone	2650[4]	0.45	3.95E-4	4.5[1]	900	1.25E-6
Water	-	1025[5]	-	-	0.65[5]	4181	1.25E-6

[1][*Scheck-Wenderoth et al.*, 2014], [2][*Clauser and Huenges*, 2013; *Schoen*, 2015; *Fuchs and Balling*, 2016b], [3][*Maystrenko and Scheck-Wenderoth*, 2013], [4][*Yegorova et al.*, 2007], [5][*Luijendijk et al.*, 2011a], [6]Values assumed of literature [*Revil and Cathles*, 1999; *Luijendijk et al.*, 2011a; *Schoen*, 2015]

2.4 Organic maturity - vitrinite reflectance

Vitrinite reflectance is chosen for modeling organic maturation. Two different vitrinite reflectance units were equally used in this study: maximum reflectance (R_{max} [%]) and random reflectance (R_o [%]). For calculating vitrinite reflectance, we applied the kinetic model EASY%R_o by *Sweeney and Burnham* [1990], which uses temperature and time as input. The method validity ranges from R_o 0.3 to 4.5 % [*Sweeney and Burnham*, 1990].

2.5 Model-data comparison

We calibrated the results of our thermal history model to match observed present-day subsurface temperatures and organic maturity data. For a first order comparison, subsurface temperature and organic maturity of the SPBA were used [*Doornenbal and Stevenson*, 2010].

2.5.1 Subsurface temperature data

Subsurface temperature datasets in 1000 (Figure 4), 2000 and 3000 m depth are available in the SPBA. We digitized the datasets of 1000 and 3000 m depth. These datasets are mostly based on interpolated borehole temperature data.

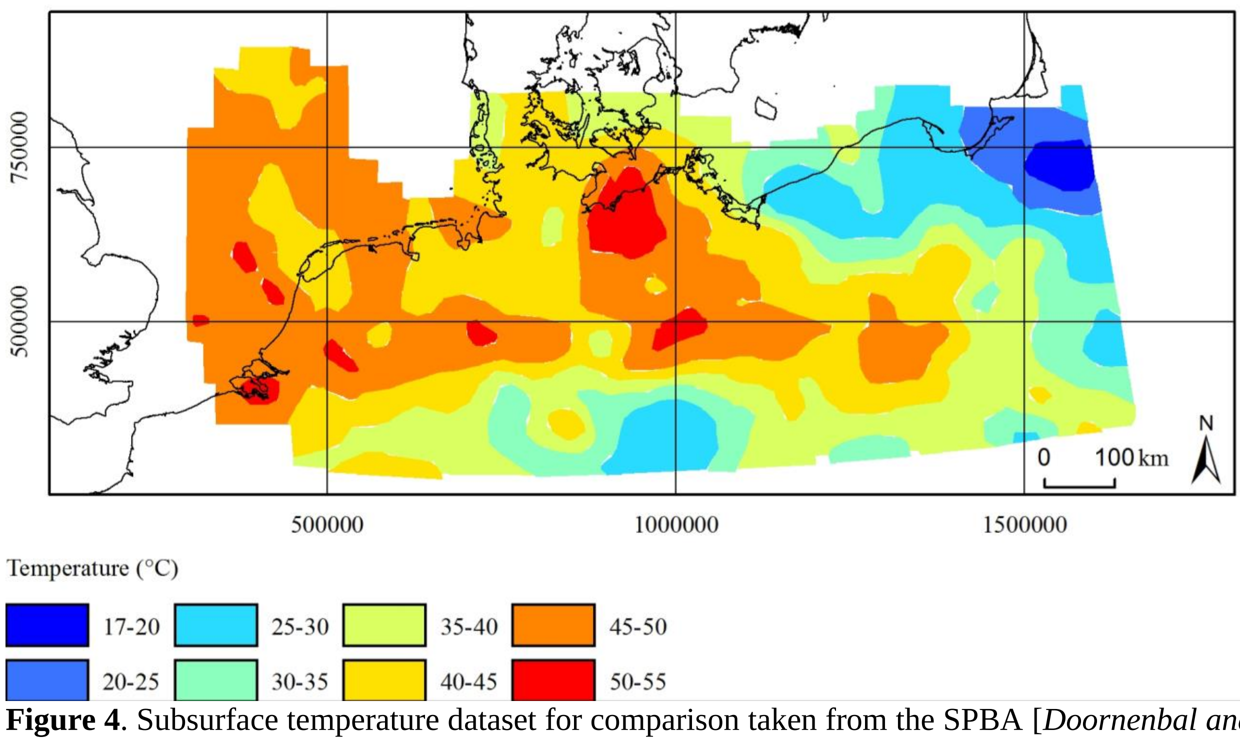

Figure 4. Subsurface temperature dataset for comparison taken from the SPBA [*Doornenbal and Stevenson*, 2010] at 1000 m depth with localized heat and cold centers based on interpolation of borehole data.

Scheck-Wenderoth and Maystrenko [2013] provide modeled subsurface temperature data in 3000 and 8000 m depth, which is based on the already mentioned lithosphere-scale regional 3D structural model [*Maystrenko and Scheck-Wenderoth*, 2013]. The subsurface temperature data of 3000 m [*Scheck-Wenderoth and Maystrenko*, 2013] were used for validating our model results, when local comparison between the SPBA and our model in 3000 m depth showed high deviations. The subsurface temperatures in 8000 m depth were the only datasets used for calibrating our model in depths deeper than 6000 m.

Additionally, we compared our dataset to the heat model of GEOELEC [*Limberger*, 2014], which is derived from data acquired in basins of hydrocarbon exploration, including borehole and calibrated data.

2.5.2 Organic maturity - vitrinite reflectance data

One vitrinite reflectance dataset of the top Carboniferous is available in the SPBA [*Doornenbal and Stevenson*, 2010], which is based on interpolation of measured borehole data (Figure 5). We fitted our lithological parameters by comparing our vitrinite reflectance model of the base of the Upper Rotliegend to the data of the SPBA of the top Carboniferous.

Further, for basins deeper than 5000 m, we used more local datasets for fitting our vitrinite reflectance of the Upper Rotliegend. These datasets are vitrinite reflectance compilations of the south of the Elbe [*Koch et al.*, 1997], of Bramsche in the Lower Saxony Basin [*Teichmueller et al.*, 1979], West Netherland Basin [*NLOG*, 2016], the north of the Elbe of the Glueckstadt Graben [*Rodon and Littke*, 2005], Poland [*Botor et al.*, 2013] and the western part of the Southern Permian Basin [*Gerling et al.*, 1999].

Additionally, we compared our vitrinite reflectance model results to measured vitrinite reflectance borehole and subcrop data of the literature for the Norwegian-Danish Basin [*Japsen et al.*, 2007], area around the Glueckstadt Graben [*Rodon and Littke*, 2005], northwest of Poland including the Pomeranian Trough as well as Pomeranian Swell [*Resak et al.*, 2008] and for the West Netherlands Basin [*Green*, 1992; *Integrated Geochemical Interpretation Ltd.*, 1996; *Luijendijk et al.*, 2011a; *NLOG*, 2016].

In addition, an alternative model with different lithological model input [*Luijendijk et al.*, 2011a] was tested.

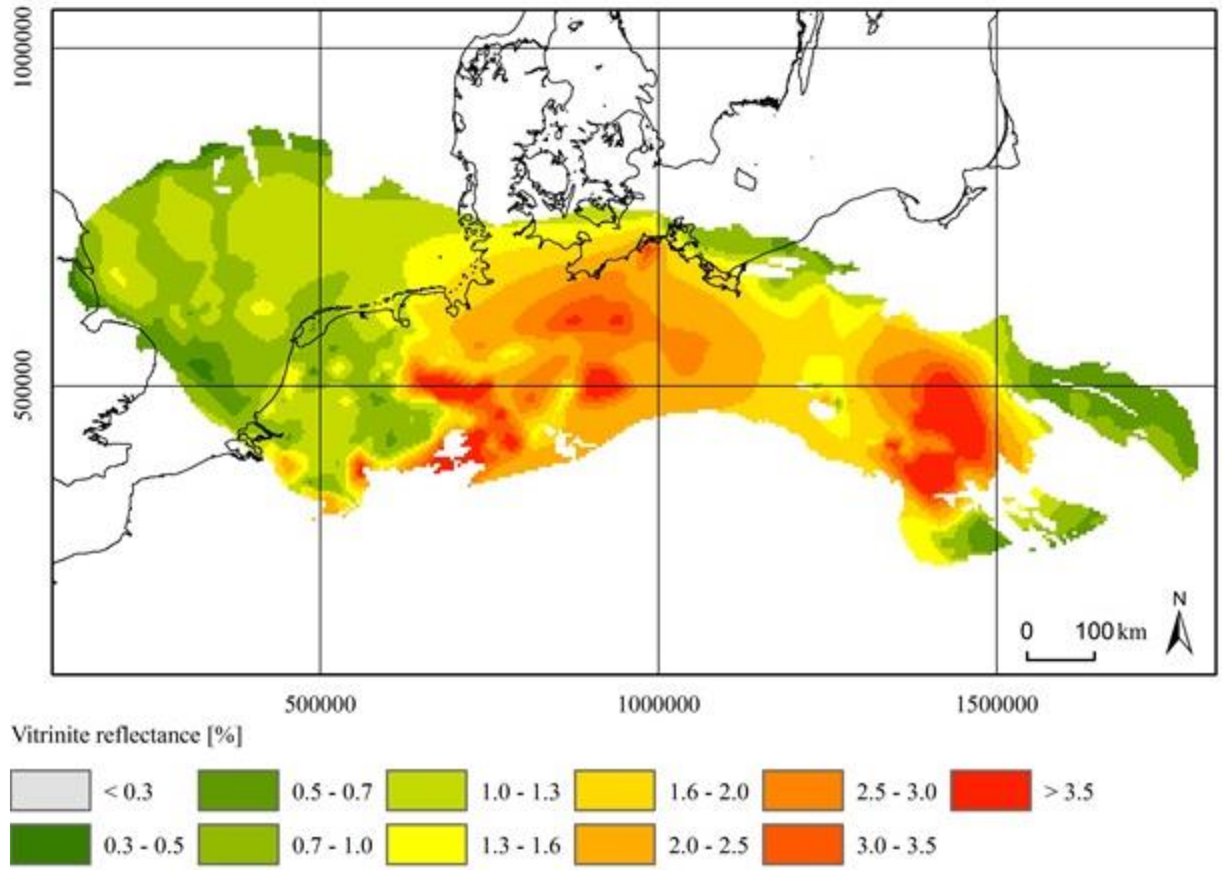

Figure 5. Vitrinite reflectance dataset from the top of the Carboniferous by the SPBA [*Doornenbal and Stevenson*, 2010] based on interpolation between borehole data points.

2.6 Model setup of sensitivity analysis

We calculated arithmetic average thickness values of the CEBS (Table 3) and modeled three boreholes with different lithological parameter sets (Table 4). Model a is the receipt dataset. The model sp is characterized by decreased surface porosity values compared to model a. The model c, compressibility, designates doubled compressibility values compared to model a. Other model properties are taken from the initial model (Table 2).

Table 3. Average thickness of the Central European Basin System

Stratigraphic unit	Quaternary (Qua)	Tertiary (Ter)	Upper Cretaceous (UCr)	Lower Cretaceous (LCr)	Upper Jurassic (UJu)	Middle Jurassic (MJu)
Average Thickness[1] (m)	162	451	585	133	390	205
Stratigraphic unit	Lower Jurassic (LJu)	Upper Triassic (UTr)	Middle Triassic (MTr)	Lower Triassic (LTr)	Zechstein (Ze)	Upper Rotliegend (Rot)
Average Thickness[1] (m)	330	551	523	552	633	398

[1]Based on SPBA dataset [*Doornenbal and Stevenson*, 2010]

Table 4. Model parameters for model a, sp, c, hp; other values according to Table 2

	Rock properties of model a			Model sp	Model c	Model hp
Stratigraphic unit	Surface Porosity (%)	Compressibility (m^{-1})	Thermal Conductivity ($W\ m^{-1}K^{-1}$)	Surface Porosity (%)	Compressibility (m^{-1})	Heat Production ($W\ m^{-3}$)
Quaternary	0.40	4.00E-4	4.0	0.2	8.00E-4	1.25E-7
Tertiary	0.40	4.00E-4	4.0	0.2	8.00E-4	1.25E-7
Upper Cretaceous	0.50	4.00E-4	3.0	0.25	8.00E-4	1.25E-7
Lower Cretaceous	0.40	2.50E-4	3.0	0.2	5.00E-4	1.25E-7
Upper Jurassic	0.40	2.50E-4	3.0	0.2	5.00E-4	1.25E-7
Middle Jurassic	0.40	2.50E-4	3.0	0.2	5.00E-4	1.25E-7
Lower Jurassic	0.40	2.50E-4	3.0	0.2	5.00E-4	1.25E-7
Upper Triassic	0.20	2.50E-4	3.5	0.1	5.00E-4	1.25E-7
Middle Triassic	0.50	4.00E-4	3.5	0.25	8.00E-4	1.25E-7
Lower Triassic	0.35	2.50E-4	3.5	0.175	5.00E-4	1.25E-7
Zechstein	0.25	4.00E-6	5	0.125	8.00E-6	1.25E-7
Upper Rotliegend	0.40	8.00E-4	4.8	0.2	1.60E-3	1.25E-7

3 Results

3.1 Comparison of modeled and measured temperature data

3.1.1 Initial model

For estimating vitrinite reflectance values, first an approximation of subsurface temperatures is necessary. For our initial model, the average absolute difference between modeled temperatures and measured temperatures [*Doornenbal and Stevenson*, 2010] is 5.8 °C. 50 % of the data points lie between -7.7 to 4.1 °C with a skewness trending to lower temperatures (Figure 6). Our initial model overestimates temperatures in basins with high total thickness values and in contrast, underestimates temperatures in basins with low total thickness values. Besides, our model overestimates temperatures in the East European Craton.

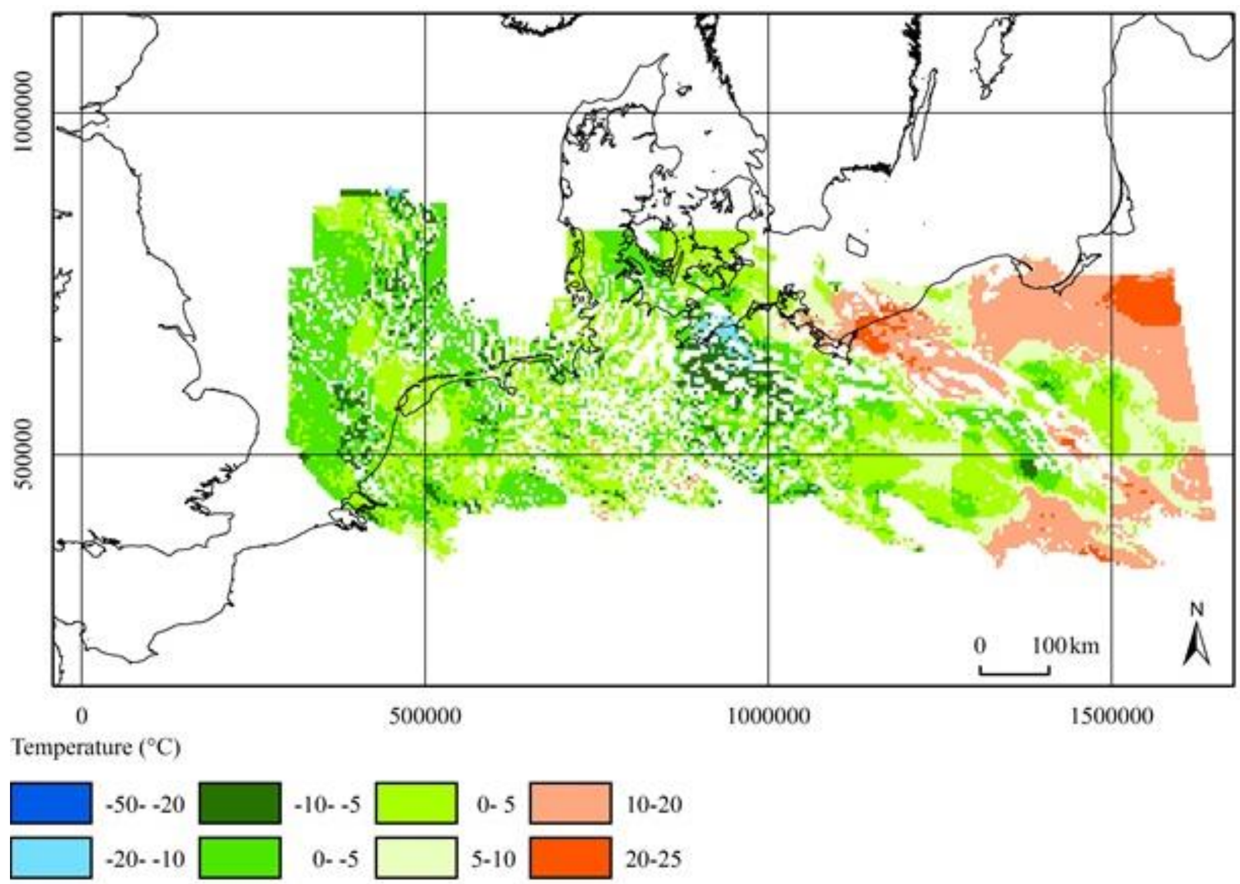

Figure 6. Comparison of our initial modeled temperatures and observed temperatures in boreholes [*Doornenbal and Stevenson*, 2010] at 1000 m depth. The temperatures of the SPBA were subtracted from our model. Green areas display temperature differences below 10 °C between both models. Red areas show that the temperatures of our model are higher, while blue areas show that temperatures are lower.

3.1.2 Sensitivity analysis

The modeled temperatures are sensitive to changes in surface porosity, compressibility and the resulting porosity, since these parameters influence the thermal conductivity of the sedimentary rocks. At the top of the modeled boreholes of the sensitivity analysis (Figure 7; Table 4), the influence of surface porosity on resulting porosity is higher than the influence of compressibility. Compressibility becomes more important with increasing depth. The Zechstein formation shows an anomaly for the reason that the initial compressibility value of this formation is very low and doubling compressibility produces nearly no change in porosity. For the Upper Rotliegend, no difference between the three models a, sp and c in porosity are observable, which starts at around 5500 to 6000 m depth. This effect on porosity in large depths is a consequence of the usage of equation 1 for calculating porosities, seeing that in these depths porosity values below 1% are assumed already in model a. Model sp and c just decrease porosity further.

The differences of porosity between the models a, sp and c translate into thermal conductivity in the form that model sp shows the highest thermal conductivity at shallow depths, as well at the Zechstein formation (Figure 7). The rest of the lithologies show for thermal conductivity more or less similar behavior.

The relation between the lowest temperatures of model sp of all three models at the bottom of the borehole is a result of the aforementioned high thermal conductivity values of model sp at the top of the borehole and of the Zechstein formation. This is due to the reason that the surface temperature and heat flux boundary condition in combination with higher thermal conductivity values lead to cooling between the boundaries compared to lower thermal conductivity. Nevertheless, the temperatures at the top of the borehole are strongly influenced by the surface boundary condition.

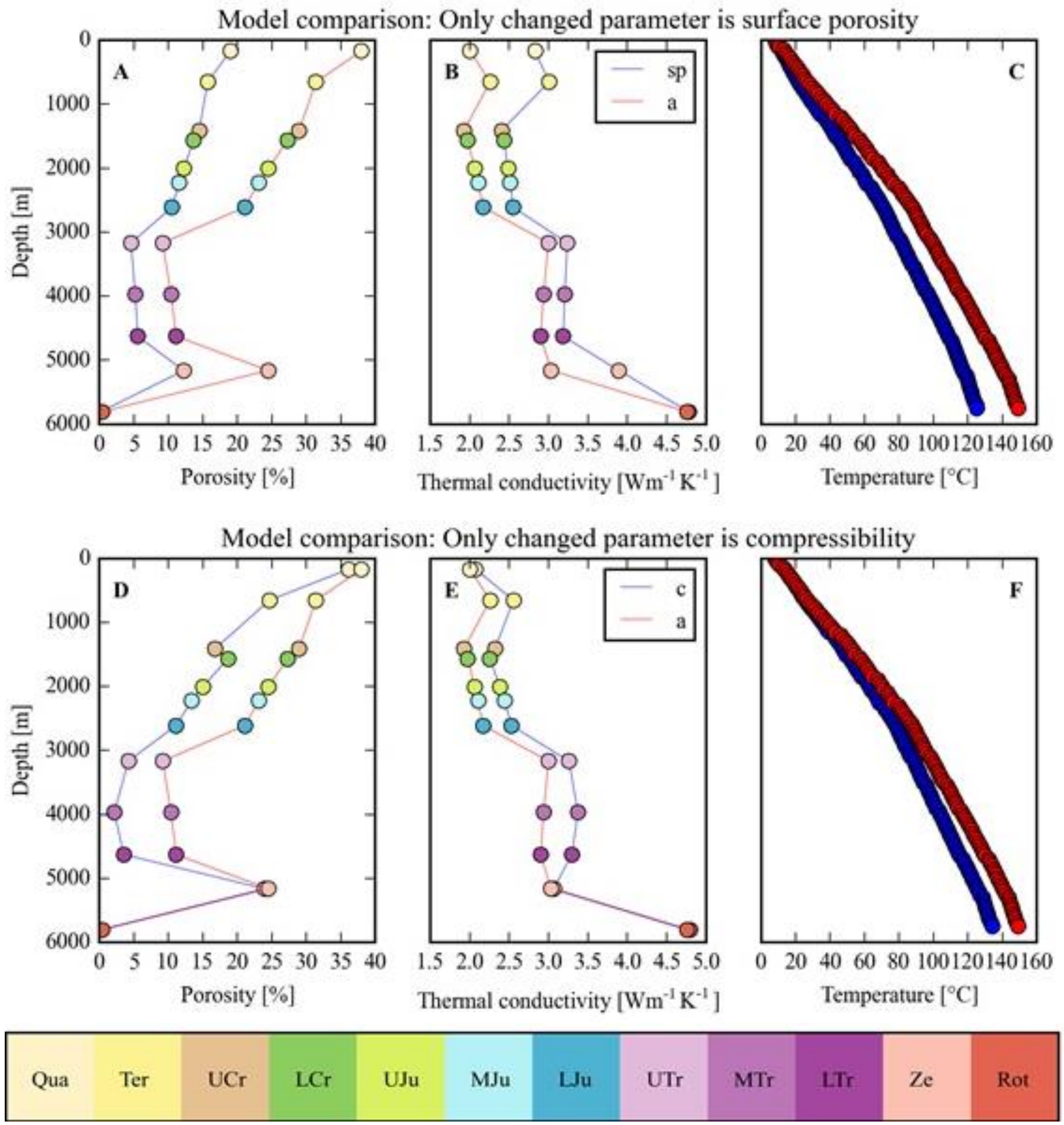

Figure 7. Three models with different rock parameters are presented on these graphs (Table 4). Model a is the receipt model based on the average thickness of the SPBA (Table 3). For model sp, the values for surface porosity were halved. For model c, the values for compressibility were doubled. The models a and sp are compared in plot A in their porosity depth relation, plot B in their thermal conductivity depth relation and in plot C in their temperate depth relation. The models a and c are compared in plot D in their porosity depth relation, plot E in their thermal conductivity depth relation and in plot F in their temperate depth relation. Model sp shows the highest thermal conductivity near the surface (B). However, this translates to overall lowest temperatures (C). For abbreviations of lithologies, see Table 3.

The variation in thermal conductivity in the model is highest for relatively old formations, because the depth of these formations varies strongly (Figure 8). However, as porosity approaches 0 % (Figure 7) and the variation of thermal conductivity is limited, because bulk thermal conductivity is then calculated by rock properties and not affected by properties of the pores fluid (Equation 1).

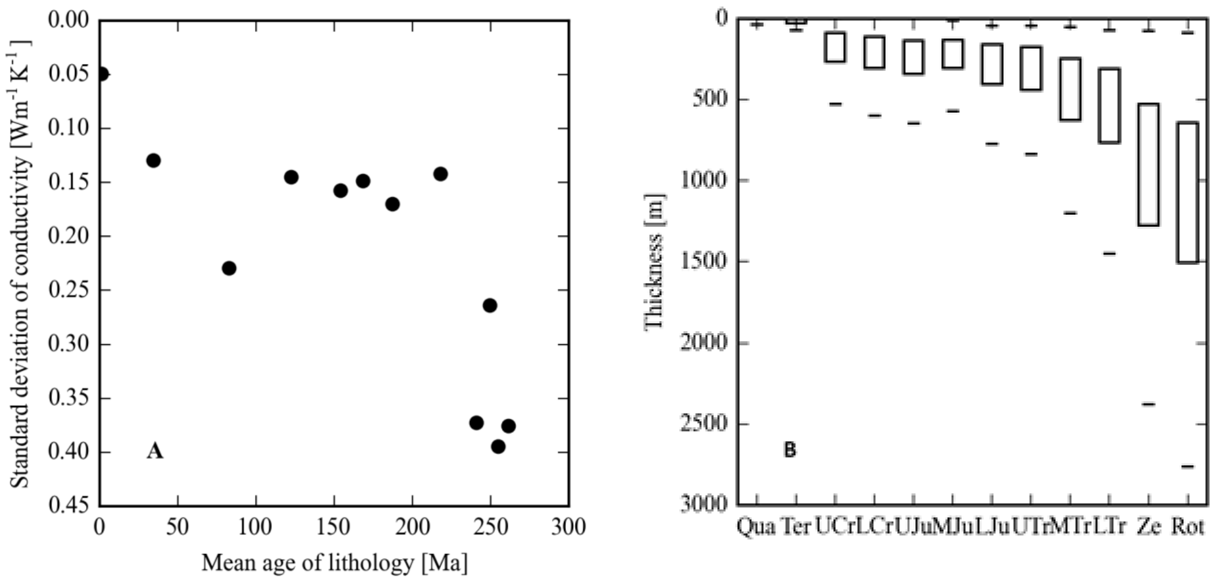

Figure 8. The relation of deviation of bulk thermal conductivity of a lithology (A) is compared to the depth of lithologies (B). Declining variations of thermal conductivity correspond with decreasing ages. This infers a gain in variation of temperatures with depth. Lithological properties are based on Table 2 and for abbreviations, see Table 3.

In Figure 9, the sensitivity of modeled temperatures to variations in heat production is shown. The heat production of model hp is one order of magnitude lower than model a (Table 4). It is comparable to the results of model sp and c, as the temperature deviations between model hp and an increase with increasing depth.

Mainly temperature influences vitrinite reflectance, but a comparison between modeled mean vitrinite reflectance based on EASY%R_o [*Sweeney and Burnham*, 1990] and modeled mean temperatures of equal depths (Figure 10) shows that the relation between vitrinite reflectance and temperature is not linear. Additionally, the modeled average geothermal gradient reaches above 50 °C/km in deep basins from 37 °C/km in shallow areas at 1 km depth.

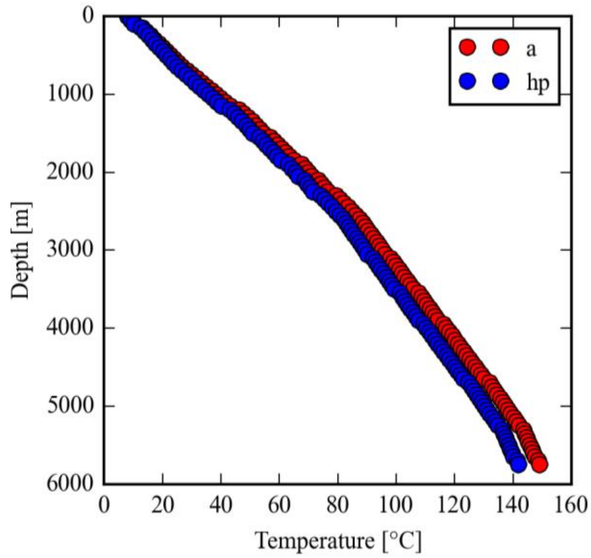

Figure 9. Subsurface temperature depth relation in a model comparison, where model hp has one-dimension lower heat productivity than model a (Table 4).

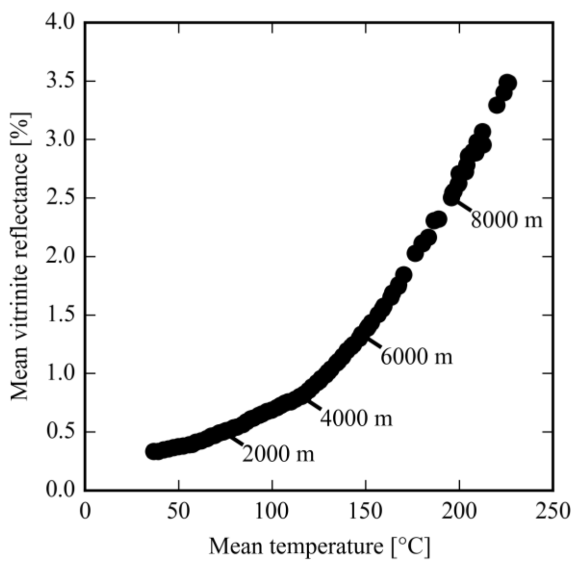

Figure 10. Temperature to vitrinite reflectance relationship showing non-linear behavior. Both values are derived as arithmetic mean for the lithologies from the total SPBA dataset with the lithological properties from Table 2. The depth of appearance is added to demonstrate that in deeper basins, vitrinite reflectance values increases stronger with increasing temperature and depth. Additionally, the geothermal gradient increases with depth also.

3.1.3 Final model

Modeled thermal conductivities are supposed to stay within reasonable bulk rock thermal conductivity values [*Clauser and Huenges*, 2013; *Fuchs et al.*, 2015; *Schoen*, 2015; *Fuchs and Balling*, 2016a], but we adjusted the rock properties by mostly considering temperature results.

On the one hand, we changed the input of surface porosity, compressibility and thermal rock conductivity of our initial model (Table 5) to reduce the misfit of the modeled subsurface temperatures. On the other hand, we changed the rock properties to decrease temperatures in basins with high thicknesses, while increasing temperatures in basins with low thicknesses.

Table 5. Final and initial lithological properties used in this study

	Final lithological properties of model			Initial lithological properties of model[1]		
Stratigraphic unit	Surface Porosity (%)	Compressibility (m^{-1})	Thermal Conductivity ($W\ m^{-1}K^{-1}$)	Surface Porosity (%)	Compressibility (m^{-1})	Thermal Conductivity ($W\ m^{-1}K^{-1}$)
Quaternary	0.35	2.50E-4	3.0	0.45	3.95E-4	3.4
Tertiary	0.35	2.50E-4	3.0	0.45	3.95E-4	3.4
Upper Cretaceous	0.5	4.00E-4	2.5	0.5	7.90E-4	3.7
Lower Cretaceous	0.4	2.50E-4	3.5	0.55	5.00E-4	3.2
Upper Jurassic	0.4	3.00E-4	3.5	0.5	5.00E-4	3.0
Middle Jurassic	0.4	3.50E-4	3.0	0.5	5.00E-4	2.1
Lower Jurassic	0.4	3.00E-4	3.0	0.5	5.00E-4	2.6
Upper Triassic	0.2	2.50E-4	3.5	0.55	5.00E-4	2.9
Middle Triassic	0.5	4.00E-4	2.5	0.5	7.90E-4	3.1
Lower Triassic	0.35	2.50E-4	3.0	0.35	5.00E-4	3.1
Zechstein	0.2	4.00E-4	4.0	0.2	7.90E-7	5.8
Upper Rotliegend	0.4	5.90E-4	4.8	0.45	3.95E-4	4.5

[1]Sources shown in Table 2

The subsurface temperatures at 1000 m depth do not deviate a lot between the initial and final model. The deviation is in the range of measurement errors [*Foerster*, 2001; *Luijendijk et al.*, 2011b]. A slight average temperature increase of the final model (Figure 11) compared to the initial model resulted: minimum, average and maximum temperatures: 30 (from initial 24), 39 (from 37) and 60 (from 57) °C.

This is because basins with lower thicknesses are more frequent, which lead to this general temperature increase. Nevertheless, basins such as Glueckstadt Graben, Polish Trough or Central Graben decreased in modeled temperature.

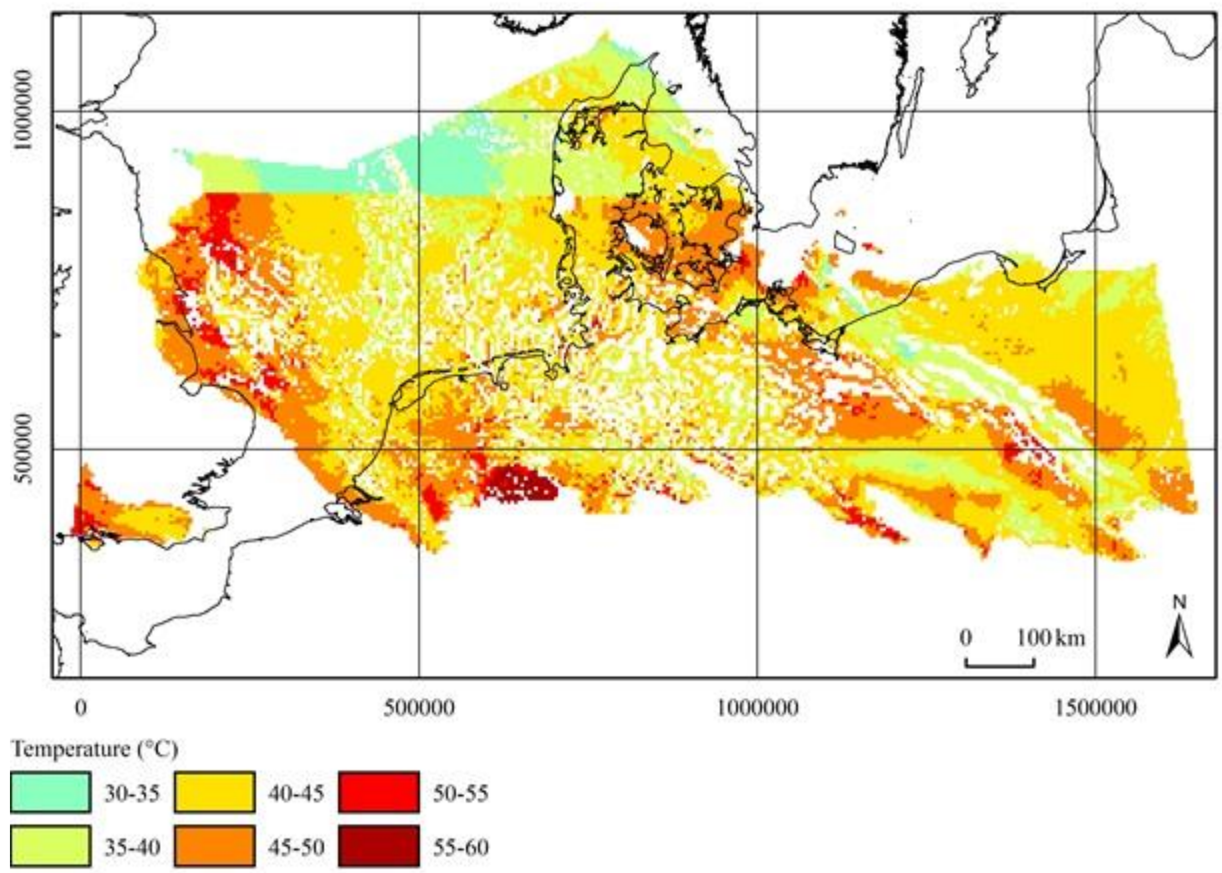

Figure 11. Final modeled temperatures at 1000 m depth with dominating temperatures in the classes between 30 to 60 °C. Observable is the input difference of the basal heat flow due to the sharp deviation in the input of basal heat flow (Figure 2). The lithological properties are based on Table 5.

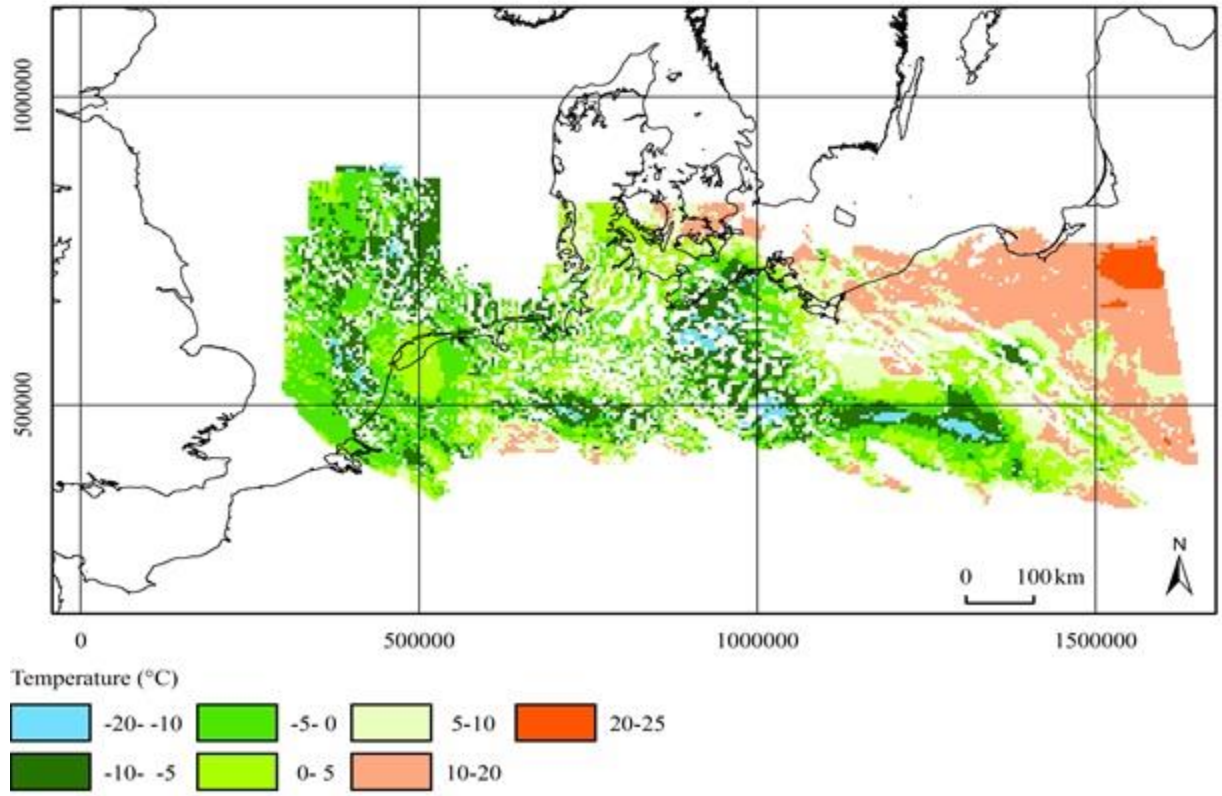

Figure 12. Subsurface temperature comparison of the model by the SPBA at 1000 m depth [*Doornenbal and Stevenson*, 2010] to our final model. The temperatures of the SPBA were subtracted from our model. Green areas display temperature differences below 10 °C between both models. Red areas show that our model is warmer, while blue areas show that our model is much cooler. The lithological properties are based on Table 5.

We modeled subsurface temperature maps at 3000 (Figure 13) and 5000 m (Figure 15) depth. Important to notice in both modeled subsurface temperature maps is that in difference to the modeled subsurface temperatures at 1000 m depth, deeper basins show lower temperatures than more shallow basins in same depth. When comparing the subsurface temperatures at 1000 (Figure 4) and 3000 m depth of the SPBA to our model results (Figures 11, 13), it is observable that our temperatures vary more lateral.

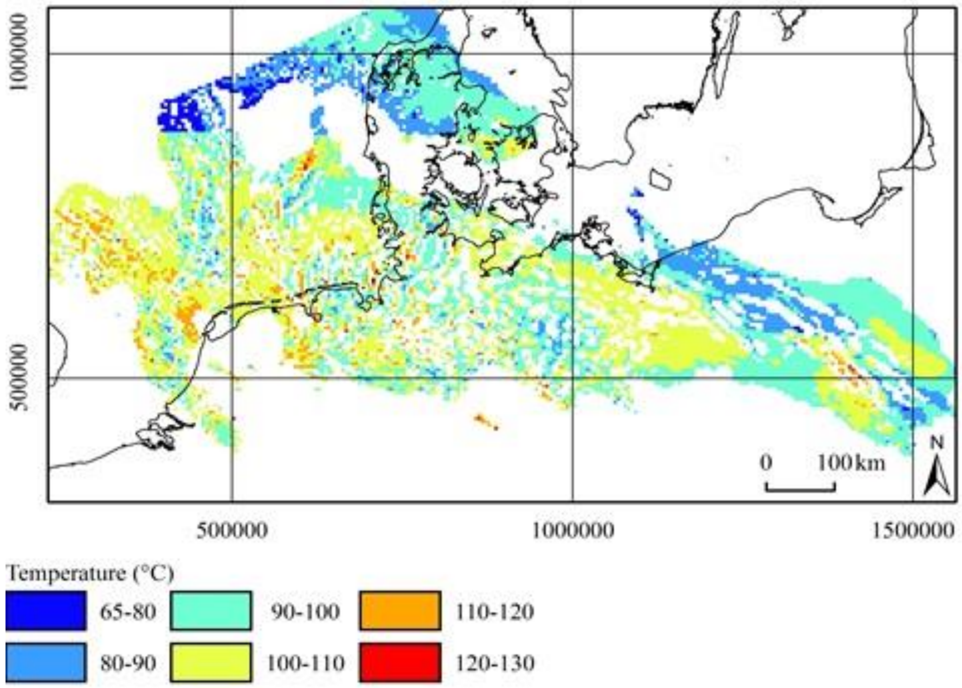

Figure 13. Modeled subsurface temperature at 3000 m depth.

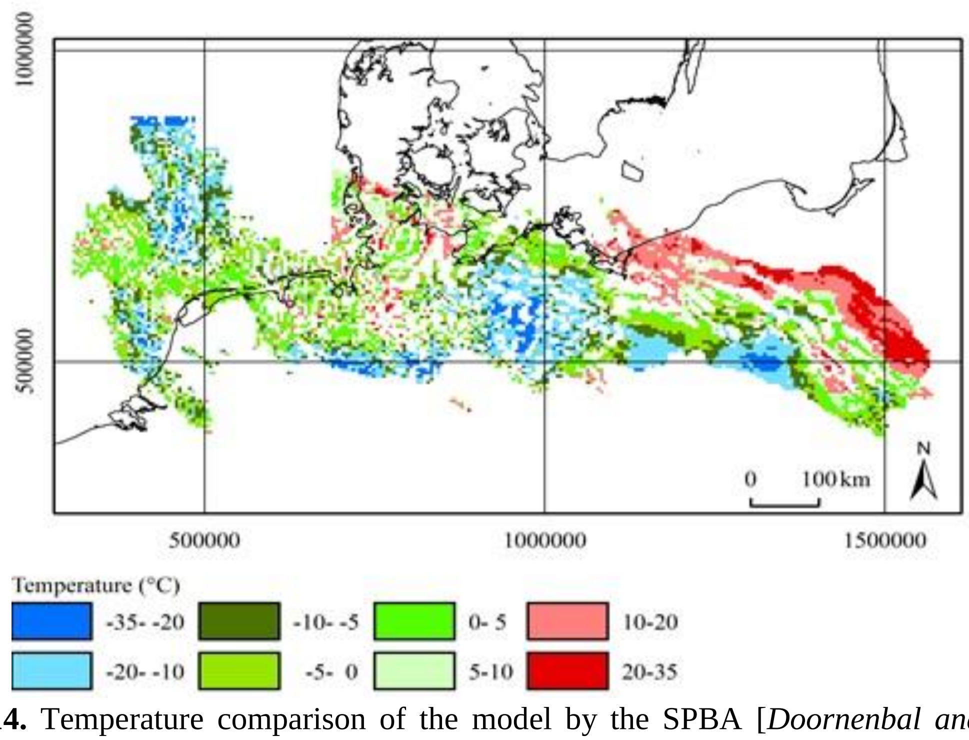

Figure 14. Temperature comparison of the model by the SPBA [*Doornenbal and Stevenson*, 2010] and our final model at 3000 m depth. The temperatures of the SPBA were subtracted from our model. Green areas display temperature differences below 10 °C between both models. Red areas show that temperatures in our model are higher, while blue areas show lower temperatures.

The data comparison at 3000 m depth of our final model versus the model by the SPBA shows that 80 % of the subsurface temperatures are below 17 °C difference between both models or 60 % below 12 °C.

Comparing our temperature model results at 3000 m depth to *Scheck-Wenderoth and Maystrenko* [2013], the deviation is mostly below 16 °C, except for the North Sea around the Central Graben, where their model shows higher temperatures up to more than 40 °C. Only in the Horngraben, our model designates higher temperature results than the model of *Scheck-Wenderoth and Maystrenko* [2013].

The subsurface temperatures of GEOELEC [*Limberger*, 2014] at 3000 and 5000 m depth are interpolated over larger areas, which is why, our model shows more lateral small-scale temperature differences. The by us modeled subsurface temperatures show minimum, arithmetic average and maximum temperatures of 105, 141 and 188 °C at 5000 m depth.

Ignoring this scale comparison difficulty and considering our model results for each sub-basin as averages, for areas in the west of the Northeast German Basin, at 3000 m depth temperatures deviate only in a range of ±10 °C. However, more or less in the east of the Oder, our model is up to 25 °C warmer. This translates into subsurface temperatures in 5000 m depth in the Polish Trough with up to 50 °C higher temperatures than the data by GEOELEC shows. For the Northeast German Basin, the GEOELEC data at 5000 m depth still shows temperatures higher up to 20 °C compared to our model, but deviation within 16 °C are achieved within the basins of Netherland. The comparison of temperatures between these models deviate below 16 °C in the Danish Basin (Figure 15).

At 8000 m depth, the modeled subsurface temperatures reach for the Glueckstadt Graben 180 to 251 °C, Horngraben 231 to 268 °C, Polish Trough 187 to 216 °C and Central Graben 175 to 222 °C. For the study area, the arithmetic average is 207 °C, but we have to admit that the modeled data points at 8000 m depth are scarce as the thickness data of the SPBA only delivers data for a few areas into a depth of 8000 m. Additionally, we excluded a lot data points when they were too close to features of salt tectonics, which are often related to deep basins. This information loss is in lower scale also valid for 5000 m depth.

Scheck-Wenderoth and Maystrenko [2013] modeled temperatures at 8000 m, which agrees to the lower temperatures by our model in the Glueckstadt Graben (circa 180 °C). Comparable subsurface temperatures at 8000 m depth are modeled for their and our model in the Polish Trough (within 16 °C). No agreement is achieved for the Horngraben, as our model results seem to be up to 50 °C higher, while our model shows for the Central Graben up to 10 to 30 °C lower temperatures.

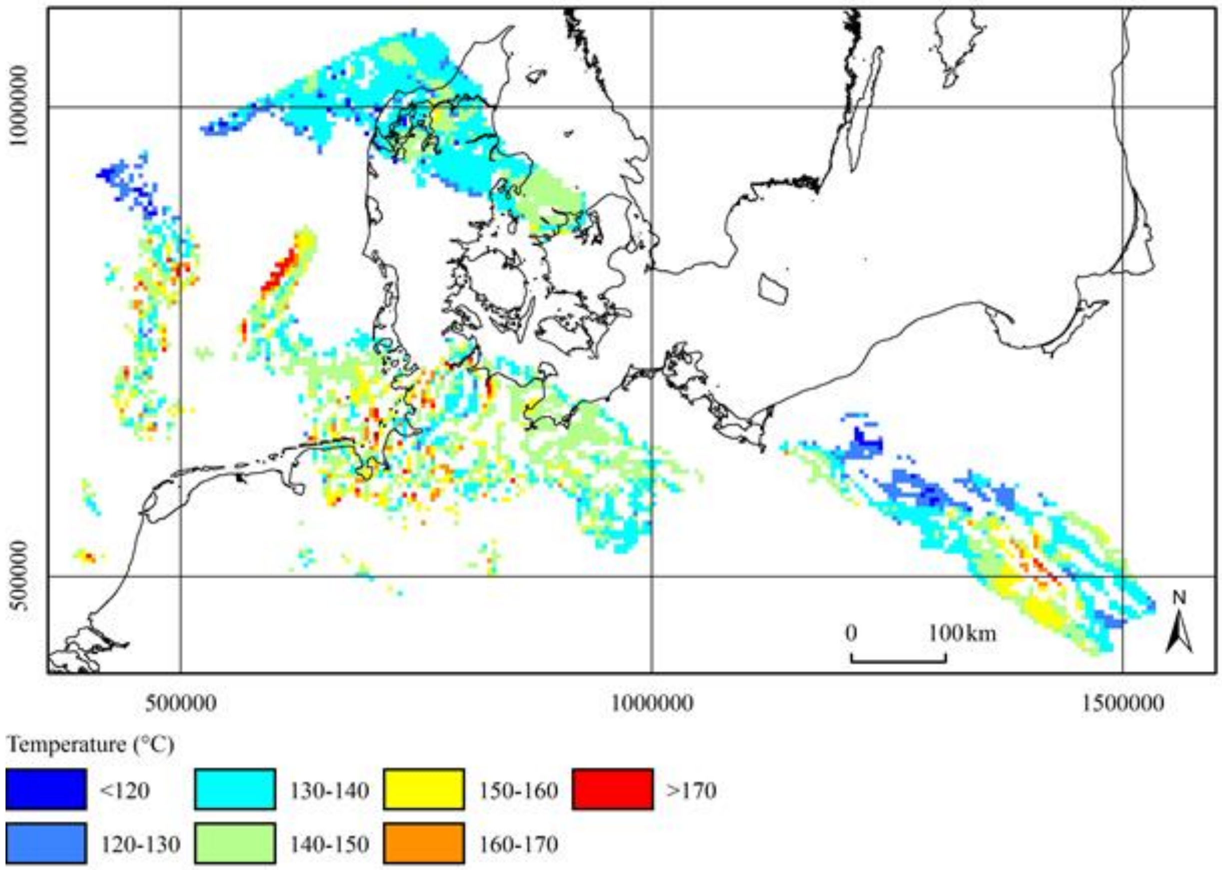

Figure 15. Modeled subsurface temperature at 5000 m depth. The scarceness of data in this map is due to the fact that the data of the SPBA only contains data in these areas to 5000 m depth and salt structures were excluded [*Doornenbal and Stevenson*, 2010].

3.2 Comparison of modeled and measured vitrinite reflectance data

3.2.1 Large scale

When comparing our vitrinite reflectance model (Figure 16) results to the interpolated datasets referred to in chapter 2.5.2, it is observable that large modeled vitrinite reflectance deviations differ mainly in deep basins (Figure 17). Around 50 % of the modeled vitrinite reflectance data (Figure 16) lies within 0.4 % vitrinite reflectance difference compared to the data of the SPBA (Figure 5).

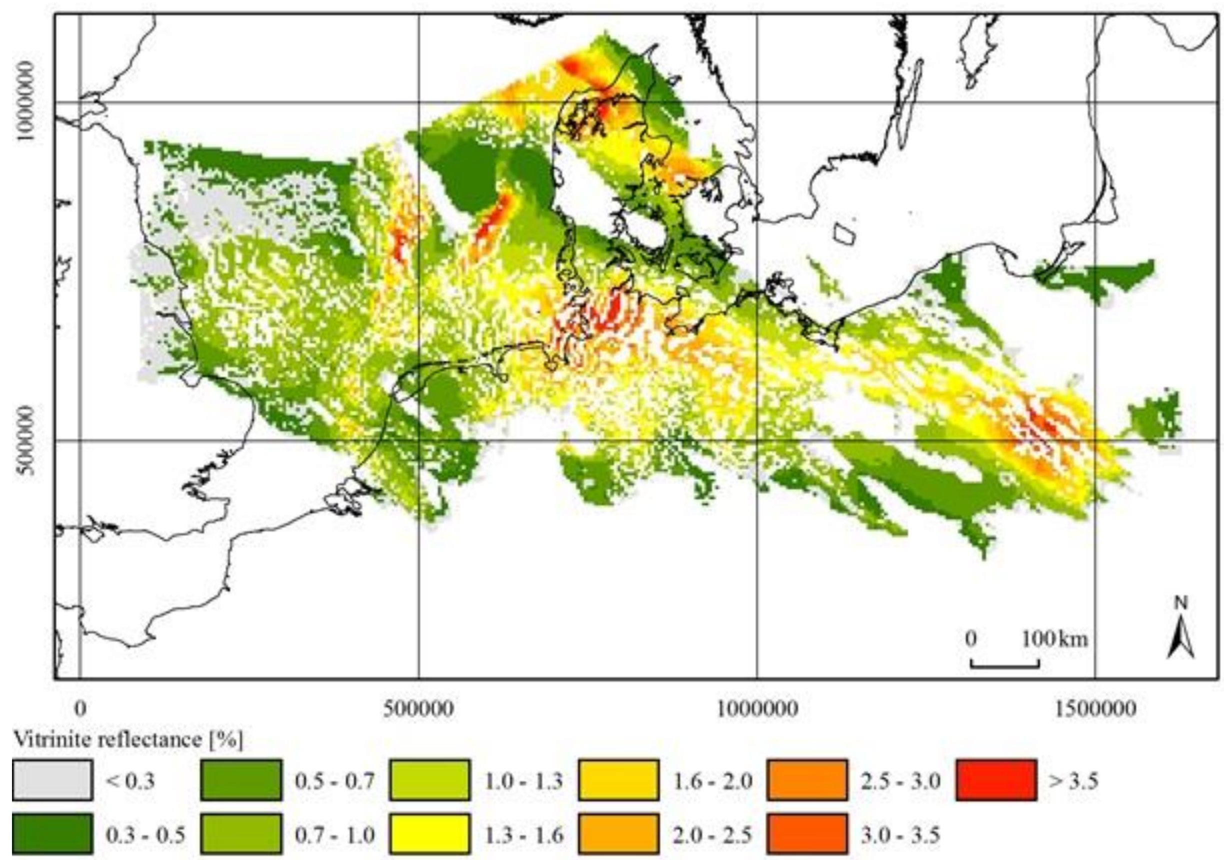

Figure 16. Modeled vitrinite reflectance at the bottom of the Upper Rotliegend formation. Grey areas designate values below the lower limit of EASY%R_o.

As expectable, the SPBA (Figure 5) and our (Figure 11) subsurface temperature model show that heat centers at 1000 m depth are not equal to modeled high vitrinite reflectance values. Nevertheless, high vitrinite reflectance values of our model coincides with the deep basins Glueckstadt Graben, Polish Trough, Horngraben, Danish Basin and Central Graben. This relation is not the case for the model by the SPBA (Figure 5).

The model by *Rodon and Littke* [2005] is also limited to the upper limit of EASY%R_o. Our modeled top of Middle Triassic shows for the center of the Glueckstadt Graben up to 0.5 % lower vitrinite reflectance than their model for the base of Keuper formation. For the area around the Glueckstadt Graben, the misfit between these two models is mostly lower than 0.5 % vitrinite reflectance.

The high vitrinite reflectance values for deep areas in the Glueckstadt Graben of *Rodon and Littke* [2005] and our model demonstrate that the vitrinite reflectance model of the SPBA does not consider data from higher depths of basins (Figure 17). Else, for the area west of the Glueckstadt Graben, this study estimates comparable results to the SPBA.

However, nearly no similarity was found between the SPBA and our model in Northeast German Basin, central Germany and southwest Poland (Figure 17), when comparing modeled values of base of Upper Rotliegend to the top Carboniferous.

In contrast, our model agrees to the isoreflectance data by *Koch et al.* [1997] for the base Zechstein formation in the area between the Ems and Oder. Besides, our modeled maturity of the Polish Trough shows slightly lower or equal maturity compared to the SPBA in lower depth areas of the Polish Trough. In higher depths, the isoreflectance by *Botor et al.* [2013] of the top Carboniferous agrees to our model results for the Polish Trough.

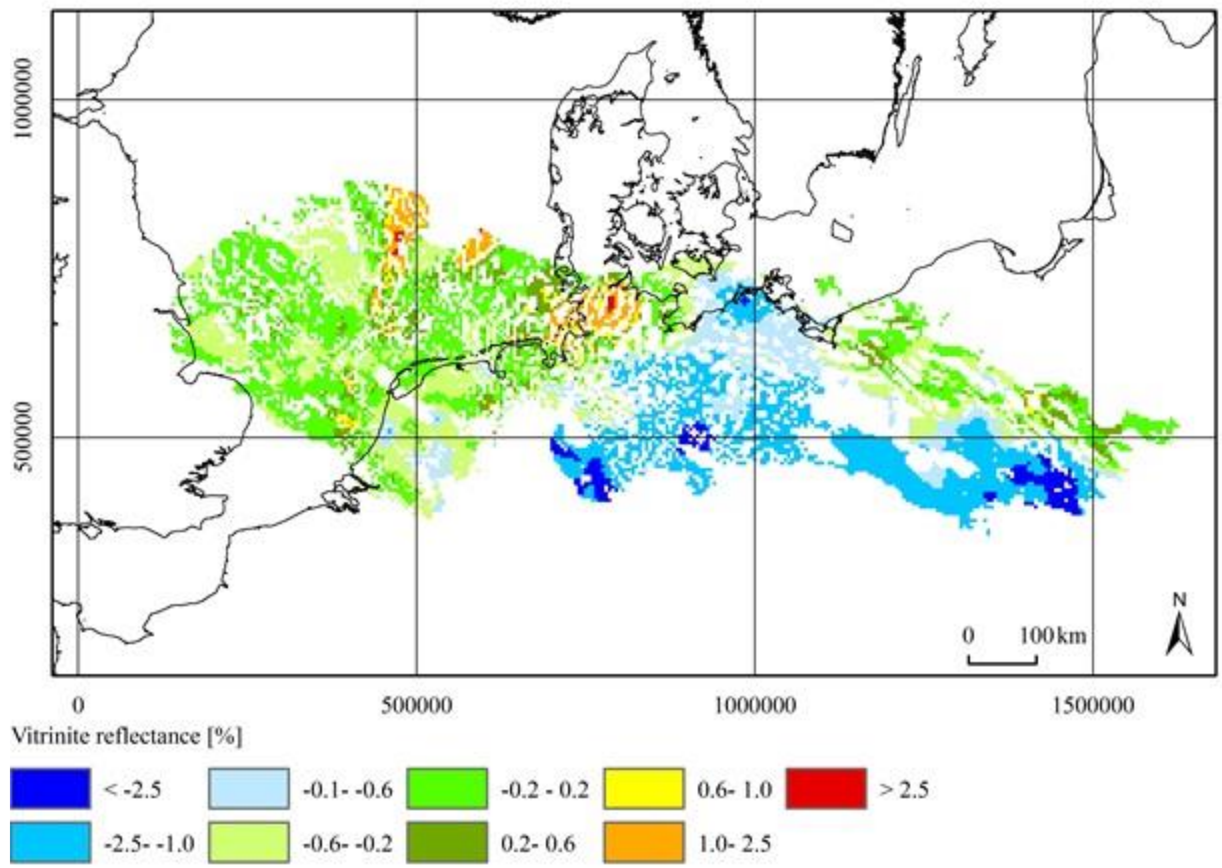

Figure 17. Vitrinite reflectance comparison of base of Upper Rotliegend to interpolated vitrinite reflectance model of the top of the Carboniferous of the SPBA (Figure 5), which is subtracted from our final model of the base of Upper Rotliegend (Table 5). Green shows area with acceptable agreement between both models. Blue indicates that the final model designates lower vitrinite reflectance values compared to the SPBA, while yellow to red shows that our model estimates higher vitrinite reflectance values. In general, our model should show lower or equal vitrinite reflectance values as we do not consider external heat sources. If this is not the case, either model assumptions are wrong or the data points for interpolation of the SPBA are not valid for this single cell. If our model shows strong lower values than the SPBA, external heat sources are assumable. Areas below the lower limit of EASY%R_o were excluded. In this study, the large blue area is referred to as pre-Permian maturity.

3.2.2 Local scale: West-Netherlands Basin and the Glueckstadt Graben

Differences in organic maturity between our model and the data by *NLOG* [2016] are observable in Figure 18. For some areas the deviation in vitrinite reflectance exceeds 1 %. In general, both datasets show elevated values for deeper parts of the study area.

When comparing our modeled vitrinite reflectance data to isoreflectance data of Bramsche by *Teichmueller et al.* [1979], we fail to predict correct values (Figure 18). Even if one would add Upper Rotliegend, the difference in vitrinite reflectance would largely stay between 1 to 4 %.

Going more into detail with comparing our model results to measured borehole data, modeled temperature gradient decrease nearly constantly without large variation in steepness (Figure 19, 20). Comparing the shape of the temperature depth curve of the Glueckstadt Graben boreholes to the West Netherlands Basin (Figure 19, 20), a curvier form is noticeable for the temperature depth relation. This curvier form is mostly due to the higher temperature span between surface and high depths in the Glueckstadt Graben.

The modeled vitrinite reflectance values do not differ a lot from the measured vitrinite reflectance, yet the slope is slightly higher for the modeled vitrinite reflectance values compared to the measured vitrinite reflectance values for boreholes 70 and 73. Another observation is that measured vitrinite reflectance values between 1.2 to 1.6 % of boreholes 70 and 73 are not predicted by the model. Borehole 58 in Figure 21 shows agreement also in depths of 4500 to 5000 m.

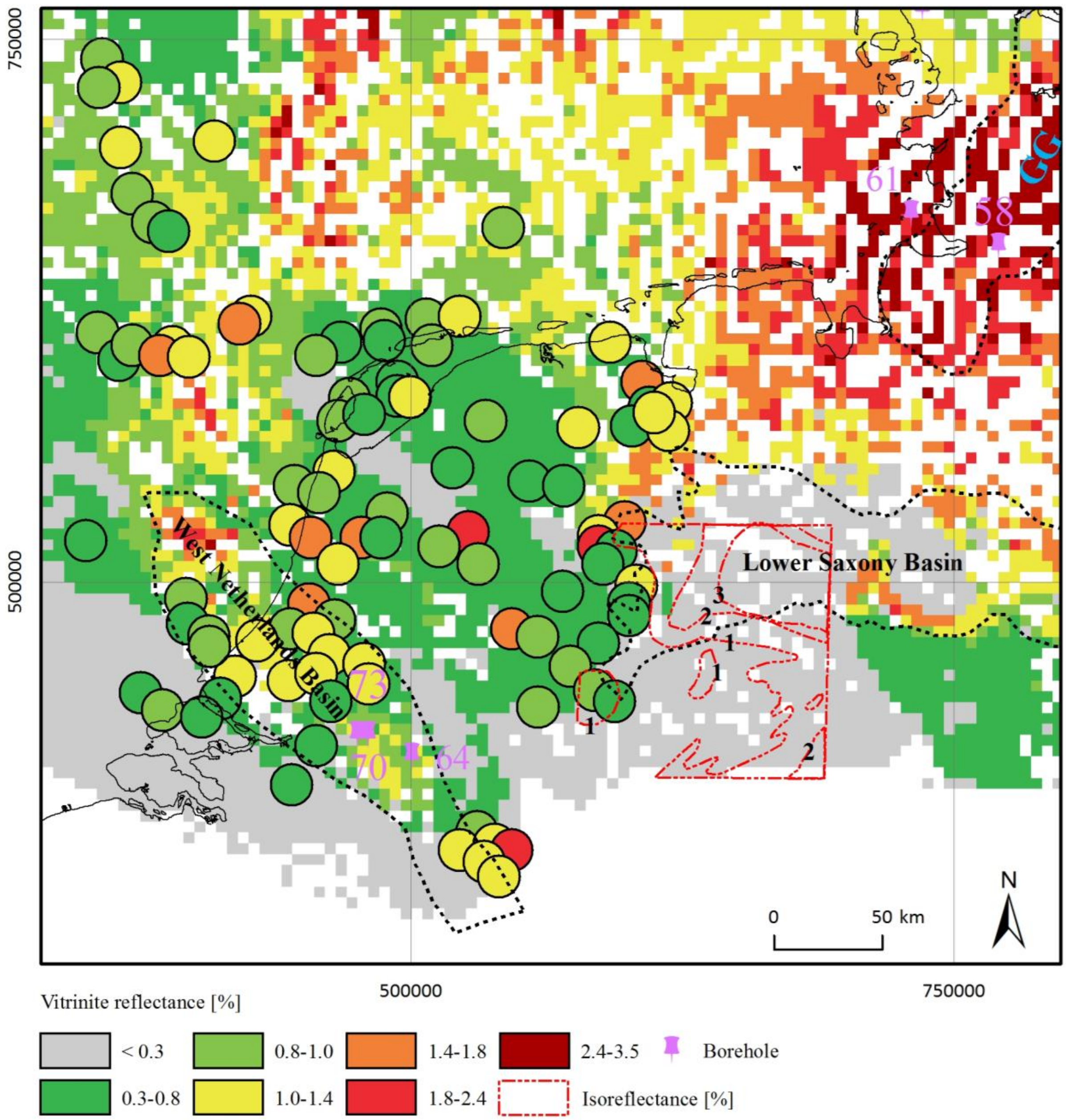

Figure 18. Vitrinite reflectance map of the top Carboniferous. Background: Modeled base of Upper Rotliegend of this study. Circles: Measured values of top of Carboniferous [*NLOG*, 2016]. Red lines: Isoreflectance adapted from *Teichmueller et al.* [1979]. Blue pushpin: marking of borehole (Figures 19 to 21). The numbers designate the modeled basal heat flow in mWm^{-2}. For vitrinite reflectance below 0.3 %, also bottom Zechstein formation data is added, when Upper Rotliegend is not preserved (Figure 1). Glueckstadt Graben (GG).

Borehole 73 – West Netherland Basin – KWK-01: A

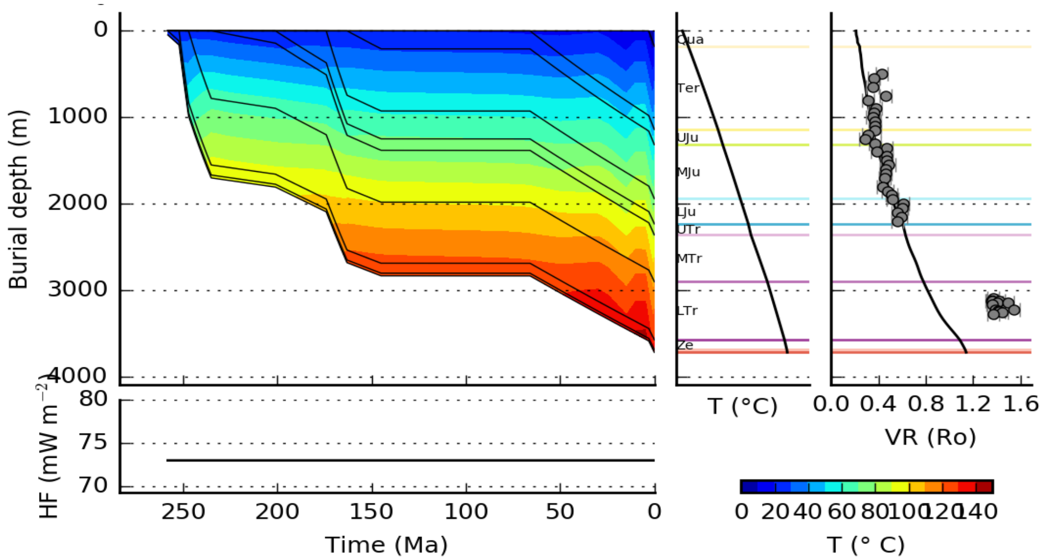

Borehole 73 – West Netherland Basin – KWK-01: B

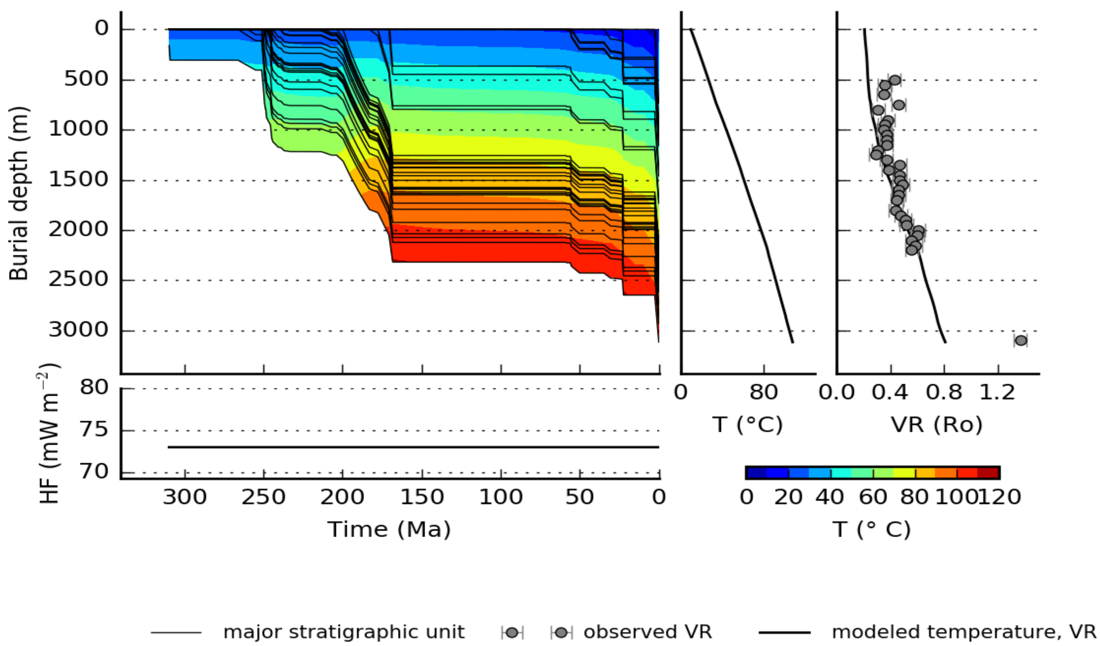

Figure 19. Thermal burial history models of A: this study and B: *Luijendijk et al.* [2011a]. Both models are with different stratigraphy and rock properties input to show the error of wrong thickness input compared to actual data. The observed vitrinite reflectance data is from *Integrated Geochemical Interpretation Ltd.* [1996] and *Luijendijk et al.* [2011a].

Borehole 64 – West Netherland Basin – HSW-01

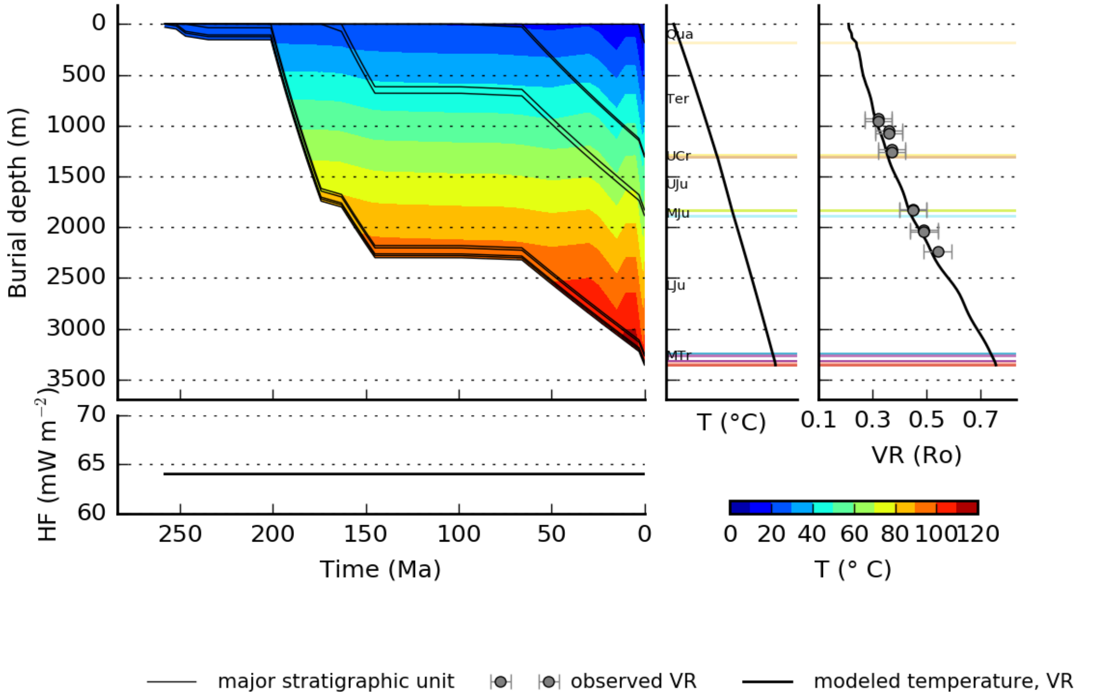

Borehole 70 – West Netherland Basin – WWK-02

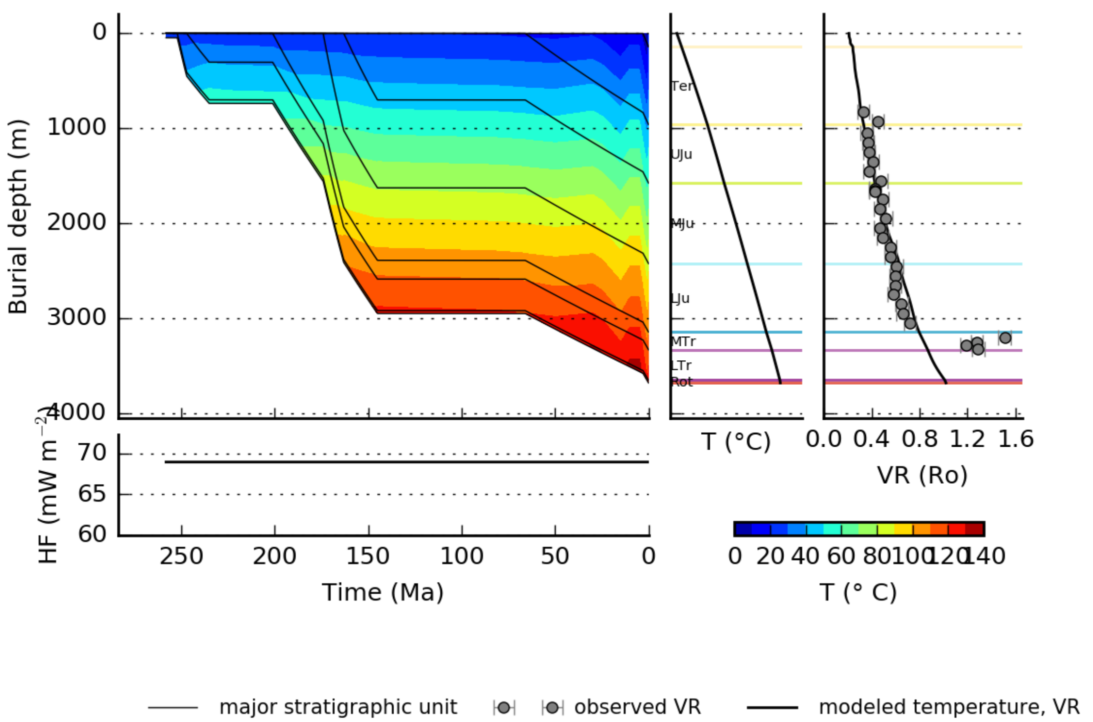

Figure 20. Thermal burial history model. Borehole 70 shows same vitrinite reflection deviation between 1.2 to 1.6 % compared to borehole 73. The observed vitrinite reflectance data is from *Integrated Geochemical Interpretation Ltd.* [1996], *Luijendijk et al.* [2011a] and [*NLOG*, 2016].

Borehole 61 – Glueckstadt Graben – Mittelplate 1

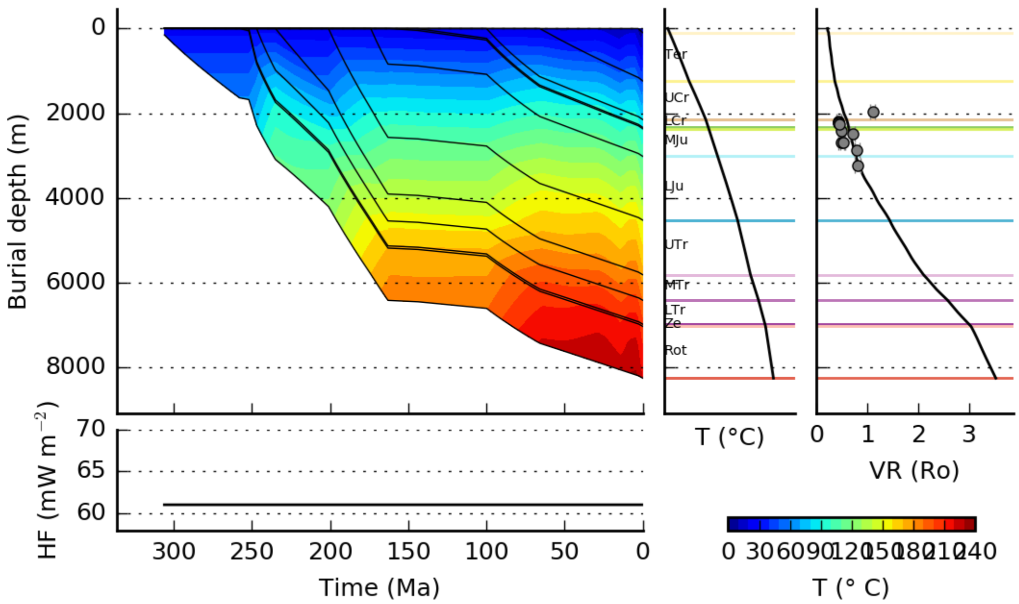

Borehole 58 – Glueckstadt Graben – Glueckstadt T1

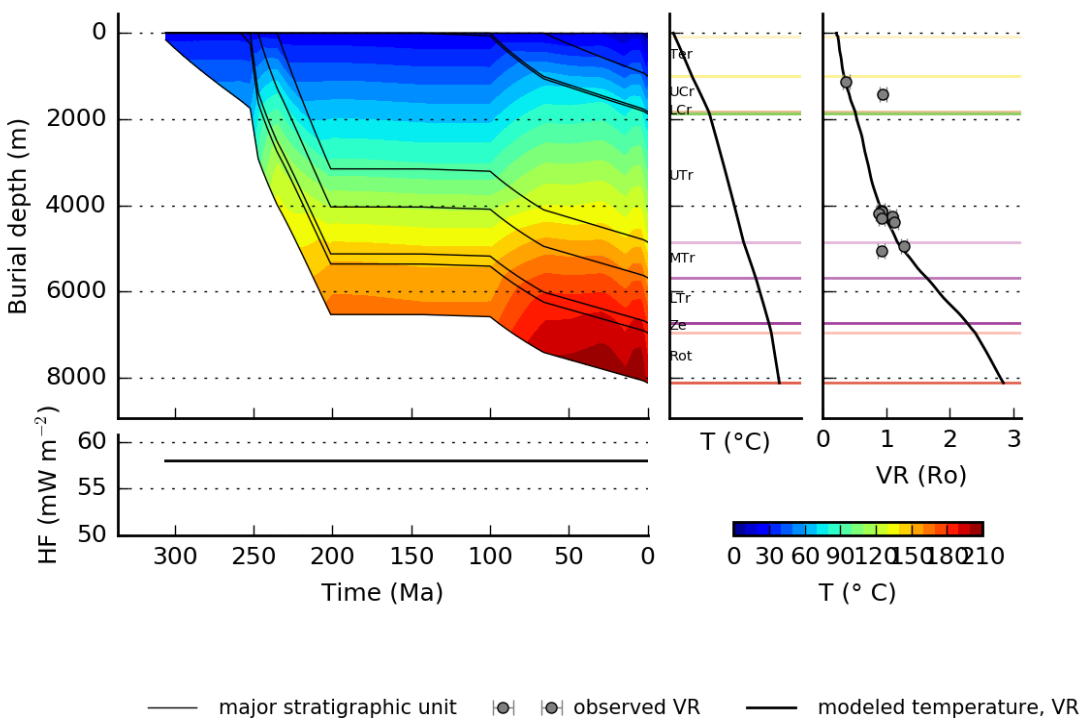

Figure 21. Thermal burial history model. These are the deepest vitrinite reflectance samples used for calibration and comparison. The observed vitrinite reflectance data from boreholes 58 and 61 are taken from *Rodon and Littke* [2005].

4 Discussion

The maturity mismatch map of Figure 17 shows differences of our model results to interpolated, measured vitrinite reflectance values by the SPBA. These differences could be the result geological events, like exhumation or elevated heat flow, which are not covered by the model of this study. However, to identify the signature of geological events we first have to exclude methodical artifacts.

Therefore, first methodical aspects of our model in respect of model limits and certainty, as well as in hindsight of current literature are discussed. Secondly, we discuss possible geological explanations for the observed misfit.

4.1 Implications due to differences of interpolated and non-interpolated datasets

The organic maturity data by the *Doornenbal and Stevenson* [2010] is interpolated from local observations of top Carboniferous, whereas our model provides 15,418 results for the bottom of Upper Rotliegend.

The formation thickness dataset that is used as input for the burial and history model perhaps contain interpolation errors of lithostratigraphic data between boreholes and seismic data [*Doornenbal and Stevenson*, 2010].

For example, the thickness data of borehole 73 (Figure 19) contains a depth error of around 650 m between the input thickness data obtained [*Doornenbal and Stevenson*, 2010] and the more accurate stratigraphy recorded in this borehole [*Integrated Geochemical Interpretation Ltd.*, 1996; *Luijendijk et al.*, 2011a; *NLOG*, 2016]. The measured vitrinite reflectance samples between 1.2 to 1.6 % are older than the Zechstein formation and are not Early Triassic. For this error, we expect a potential overestimation of maxima 0.5 % vitrinite reflectance for the bottom of the Zechstein formation, when assuming that the geothermal gradient is constant and the burial depth is corrected by 650 m. In borehole 70, a similar error of around 350 m is observable.

Another methodological reason for organic maturity mismatches in Figure 17 are erroneous interpolation of measured data by the SPBA [*Doornenbal and Stevenson*, 2010]. As the results earlier have shown, for higher depths, the organic maturity data of the SPBA is unreliable. This unreliability might be explained by the number of measurements in this depth included into the compilation of the dataset. In areas with total sediment thicknesses lower than

5000 m and in the area of the Glueckstadt Graben, the organic maturity of the SPBA agrees to *Rodon and Littke* [2005] and to our model results.

In addition, the vitrinite reflectance of the SPBA agrees in large parts with more detailed local studies of vitrinite reflectance in north central Germany [*Koch et al.*, 1997], Poland [*Botor et al.*, 2013] and the North Sea [*Gerling et al.*, 1999].

4.2 Implications and limitations of the thermal history model

The modeled organic maturity depends on reliable estimation of subsurface temperature. In this study, we modeled subsurface temperatures using estimates of thermal conductivity and thermal boundary conditions composed of surface temperature and basal heat flow. The basal heat flow boundary condition was based on a model of the present-day lithosphere by *Scheck-Wenderoth et al.* [2014], which may not be representative of the basal heat flow in geologic history.

Nevertheless, the basal heat flow prevailed largely over the modeled geologic history with only slight variations in the general setting of the CEBS, because the thickness and heat production of the lithosphere were relatively constant during the Mesozoic and Cenozoic. This is confirmed by vitrinite reflectance and apatite fission track studies, which constrain thermal history [*Rodon and Littke*, 2005; *Japsen et al.*, 2007; *Littke et al.*, 2008; *Luijendijk et al.*, 2011a; *Botor et al.*, 2013; *Sachse and Littke*, 2016].

However, the basal heat flow data by *Scheck-Wenderoth et al.* [2014] does not span over the whole study area and hence, our basal heat flow estimation for the other part of the area (Figure 2) is based on a less reliable calibration.

The significance for this study is observable in the sharp deviation of temperatures of maximum 20 °C in the North Sea (Figure 11), which coincides with a maximum deviation in basal heat flow of 27 mWm^{-2}. In most cases, the temperature differences between each side of the sharp line are below 10 °C, except for areas in the north west of the study area.

Subsequent to the uncertainty in using constant values for the basal heat flow over geologic timescale, the applied surface temperature boundary estimation (Figure 3) contains uncertainties also. This surface temperature incorporates a correction for Pleistocene influenced heat flows, since subsurface temperatures are assumed to be not in equilibrium since the

Pleistocene [*Luijendijk et al.*, 2011a; *Fuchs et al.*, 2015; *Fuchs and Balling*, 2016b]. This affects temperatures and heat flow in up to 2000 m depth according to *Majorowicz and Wybraniec* [2011].

These Pleistocene lowered heat flows potentially explain a part of the offset in subsurface temperatures in the east of Poland (Figure 12, 14), since the used Pleistocene temperature adjustment originate from Belgium and the Netherlands [*Helsen and Langenaeker*, 1999; *Luijendijk et al.*, 2011a]. Between Belgium and the east of Poland, *Majorowicz and Wybraniec* [2011] designate a difference in paleoclimate correction of around 10 mWm^{-2} in their difference map between corrected and uncorrected heat flow. As implication, the modeled temperatures from the surface up to the bottom of the boreholes are overestimated in our study for this area.

Seeing that subsurface temperature misfits in the east of Poland increase drastically with depth, we expect that the Pleistocene influence is not the only source for misestimating of temperatures in the east of Poland. *Narkiewicz et al.* [2010] assume a lower present-day basal heat flow than compared to *Scheck-Wenderoth et al.* [2014]. The heat flow by *Scheck-Wenderoth et al.* [2014] is based on an upper boundary condition of 5 °C as average of mean annual surface temperature and temperatures observed at the seafloor. The lower boundary condition is set between the conductive lithosphere and partially molten asthenosphere [*Scheck-Wenderoth et al.*, 2014]. The heat flow was calibrated against subsurface temperature measurements [*Scheck-Wenderoth and Maystrenko*, 2013]. The potential overestimation of basal heat flow may explain the overestimation of subsurface temperatures by our model.

The lower present-day basal heat flow by *Narkiewicz et al.* [2010] agrees to lower heat production in the continental crust for this area [*Jaupart et al.*, 2016] and lower heat flows in the East European Craton [*Hossein et al.*, 2006] . The radiogenic heat production being integrated into our model is slightly lower than compared to literature [*Allen and Allen*, 2005; *Scheck-Wenderoth et al.*, 2014], but in the significance analyses (Figure 9) it is observable that this parameter plays a minor role. Therefore, we simplified the input of radiogenic heat production (Table 2).

Salt tectonics and its thermal chimney effect are also not able to explain such high temperature deviations over such a wide area like in east Poland, together with the fact that we excluded most salt structures on the basis of data of the SPBA [*Doornenbal and Stevenson*, 2010]. Additionally, salt tectonics often come together with complicated local geologies, which is potentially not covered by a one-dimension model setup. Nevertheless, the chimney effect leads potentially to temperature abnormalities of up to 9 °C in distances up to 500 m to the salt body [*Jensen*, 1983] or 30 °C directly above the salt body [*Littke et al.*, 2008]. When 2000 m thick evaporites are assumed, the temperatures below the salt body are perhaps decreased by 20 to 30 °C [*Zhuo et al.*, 2016].

To explain the temperature misfit in the east of Poland, fluid flow as external heat source or sink is unlikely the cause, since transferring heat between sub-basins in such a wide area is probably excludable [*Foerster*, 2001; *Luijendijk et al.*, 2011b; *Fuchs and Balling*, 2016a]. Yet locally, e.g. in Brandenburg indications are given for fluid interactions on the thermal field [*Noack et al.*, 2012]. For the reason that the model setup consists of one-dimensional models, there is no control about any fluid movement, except when the fluids are moved within the rock column as pore fill.

This also means, that our model does not integrate any external fluid flow heat source or sink. In consequence, pressure conditions are also not considered by our study [*Allen and Allen*, 2005; *Zhang*, 2013]. There are maybe circumstances [*Zhang*, 2013], where overpressure denies compaction, yet unusual settings like fast burial are necessary to explain it, but *Nielsen et al.* [2015] argues that proposed overpressure often agree to misestimated vitrinite reflectance by EASY%R_o.

However, we derive bulk rock thermal conductivity by taking the exponential porosity-depth relation into account, for which *Bahr et al.* [2001] argues that it is an excellent first-order approximation for porosity. In contrast, the kind of sediment and local variations in a formation, such as 0 to 20 % porosity in a Zechstein formation of the same depth [*Clark*, 1986], possibly lead to misestimates [*Schoen*, 2015].

In current literature [*Scheck-Wenderoth et al.*, 2014; *Fuchs and Balling*, 2016a, 2016b], depth dependency of thermal conductivity is integrated by interpolating between well log data, but also modified by considering facies dependent thermal conductivity and literature data. However, large deviation in burial depth within one facies may lead with this approach to misestimated thermal conductivity (Figure 8). Potentially this explains, why our model produces more lateral subsurface temperature variation than the model by *Scheck-Wenderoth and Maystrenko* [2013] in basins with thicker formations. But, we do not include facies analyzes.

Moreover, this study possibly inhibits the uncertainty *Fuchs and Balling* [2016a] argue of, which states that thermal conductivity based on literature values might be more wrong than taking random values. As they advised in their publication, we calibrated the input thermal conductivity, adapted from literature, with borehole data and other models, minimizing this uncertainty as good as possible.

4.3 Organic maturity model and its relation to the thermal model

In this study, the organic maturity is assessed by modeling vitrinite reflectance modeling using modeled subsurface temperatures and time as input [*Sweeney and Burnham*, 1990]. Local studies [*Rodon and Littke*, 2005; *Botor et al.*, 2013] found a good agreement between the modeled and observed vitrinite reflectance values using the EASY%R_o method. Therefore, it is not likely that errors in the EASY%R_o algorithm are the cause for the misfit of the modeled and observed vitrinite reflectance values. However, according to *Nielsen et al.* [2015], EASY%R_o overestimates vitrinite reflectance to an amount maximal of 0.35 % in the range of 0.5 to 1.7 % R_o.

We use several different data sources for vitrinite reflectance, in which different definitions are applied, e.g. R_{max} and R_o. Additionally, rocks with different lithological properties influence the deviation of vitrinite reflection by a maximum 16 % in silt- and sandstones and 10 % in claystone compared to coal seams [*Bruns and Littke*, 2015] adding up to a potential maximum deviation of 0.72 % at 4.5 % vitrinite reflectance.

Considering the non-linear relation of temperature and vitrinite reflectance (Figure 10), it shows that estimation of temperatures in shallow basins is less likely to lead to misestimating of vitrinite reflectance than in deeper basins, because the increase of vitrinite reflectance increases more with higher temperatures.

This maybe explains the maturity misfit relation (Figure 17) in deeper basins such as Glueckstadt Graben, Horngraben or Central Graben. For instance, *Rodon and Littke* [2005] agrees to our model in lower depths and results in stronger mismatches in the center of the

Glueckstadt Graben. Besides, the uncertainty of modeled temperatures is higher at higher depths as the amount of data for calibration decreases.

In the burial and thermal history of these boreholes, the assumed surface temperature influences the isotherms directly, since the timing of the maxima and minima temperature values correspond to assumed input surface temperature time wise (Figure 3). Conclusively, our modeled maximum vitrinite reflectance values are often reached 5 million years ago when the surface temperature was warmer than during the Pleistocene and Holocene.

4.4 Lower Rotliegend volcanism

The misfit of the modeled and observed organic maturity can be partly explained by volcanic activity. For example, the Northeast German Basin shows high deviations in organic maturity.

The amounts of intrusives and extrusive volcanic rocks are dated as Lower Rotliegend [*Timmerman*, 2004; *Geißler et al.*, 2008; *Littke et al.*, 2008; *Doornenbal and Stevenson*, 2010; *Regenspurg et al.*, 2016]. Extrusive volcanic rocks are not correlated with elevated levels of vitrinite reflectance. However, intrusive rocks described by *Heeremans et al.* [2004] coincide with area, where high values of organic maturity are observed (Figure 22). Intrusives are more likely to increase basal heat flow and geothermal gradients.

Geißler et al. [2008] argue for low sedimentation rates due to (semi)arid climatic conditions and thus, a morphological stable situation. Even though, the Sadler effect [*Sadler*, 1981] was not considered in this study, different time scales and sedimentation rates were analyzed (Chapter 5) and potentially resulted in misestimating of erosion of Lower Rotliegend volcanic rocks.

Nevertheless, the supposed morphological stable situation explains, why only few sedimentary Lower Rotliegend formations are found and long lasting unconformities exist within the CEBS between Upper Rotliegend and pre-Permian [*Geißler et al.*, 2008].

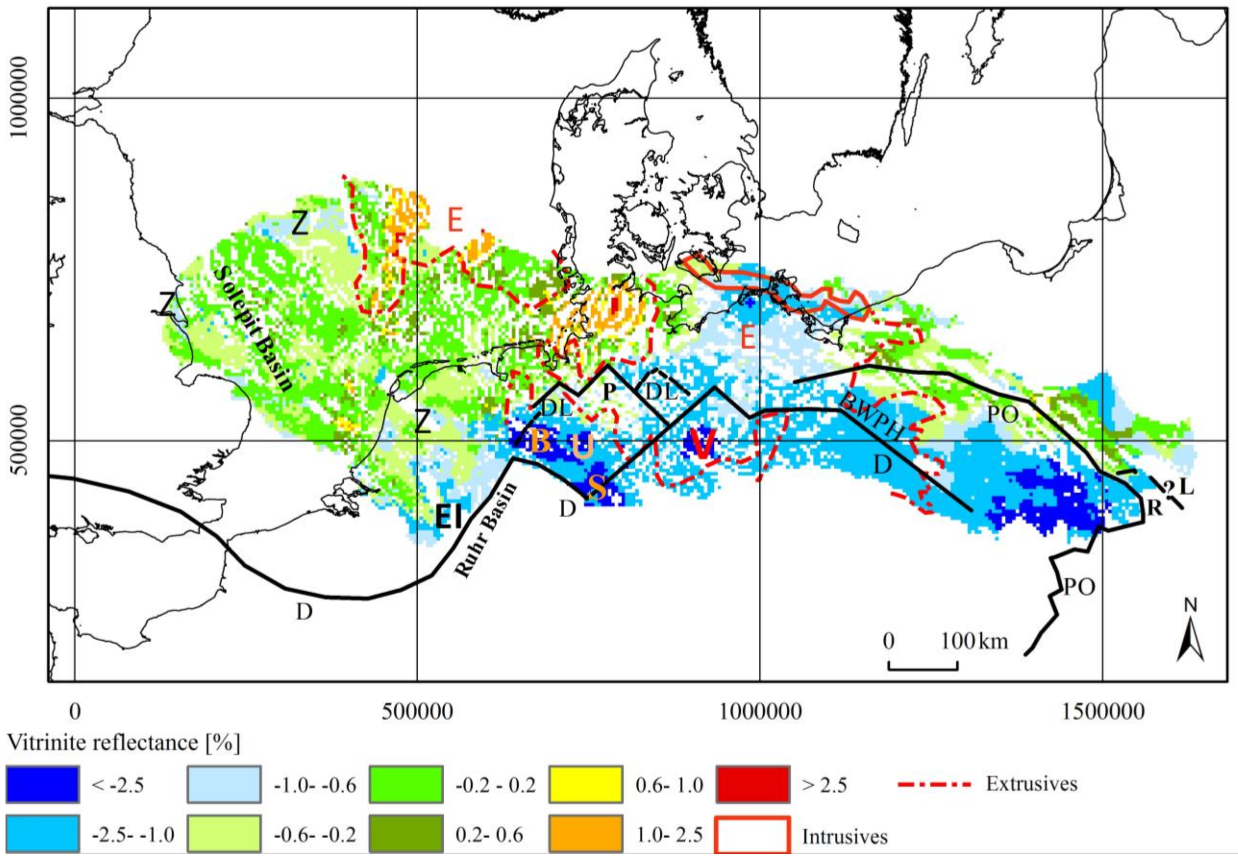

Figure 22. Vitrinite reflectance comparison of base of Upper Rotliegend to interpolated vitrinite reflectance model of the top of the Carboniferous of the SPBA [*Doornenbal and Stevenson*, 2010]. When Upper Rotliegend is not preserved, we use vitrinite reflectance of base of Zechstein formation to calculate the difference between the SPBA and our study. Blue shows underestimation by our model, while yellow to red designate overestimation. Green shows agreement to the SPBA. Intrusive and extrusive Lower Rotliegend volcanic rocks are adapted from *Heeremans et al.* [2004]. Variscan deformation fronts are adapted from *Dulce and Lewis* [2011] (DL), *Drozdzewski et al.* [2009] (D) and *Pozaryski et al.* [1992] (PO). Variscan deformation front between Lublin Basin (L) and Radom-Krasnik Block (R) is adapted from *Krzywiec et al.* [2016]. Erkelenz intrusion (EI), Bramsche Massif (B), Sollingen (S), Uchte (U), Velpke-Asse intrusion (V), Brandenburg-Wolsztyn-Pogorzela high (BWPH). The organic maturity is in thick basins such as Glueckstadt Graben, Horngraben and Central Graben are not well described in the SPBA dataset. The use of Zechstein formation (Z) lead in local occasions to strong deviations.

4.5 Exhumation

Every now and then, differences between modeled and observed organic maturities are caused by uplift and subsequent exhumation of deeper buried formations, since the eroded materials are potentially not considered in burial and thermal history models.

However, exhumation events are not modeled by this study. For example, the widespread Late Cretaceous inversion [*Kley and Voigt*, 2008] affected the Central Graben [*Gerling et al.*, 1999], the Solepit Basin [*de Jager*, 2003], the Polish Trough [*Botor et al.*, 2013] and the West Netherland Basin [*NLOG*, 2016], which still show accordance or overestimation for vitrinite reflectance compared to our model. One explanation is that the measured maximum vitrinite reflectance were reached earlier than our model results show, e.g. in the Polish Trough in the Late Cretaceous [*Botor et al.*, 2013]. Hence, burial with subsequent Late Cretaceous inversion overprinted the missing effects of the not modeled exhumation.

An organic maturity misfit example is the Lower Saxony Basin, where the Bramsche Massif is supposed to be situated (Figure 18). Higher temperatures were earlier explained by a plutonic intrusion [*Teichmueller et al.*, 1979], but recently deep burial and following exhumation in Late Cretaceous in combination with uplifted parts of the lower crust is argued for [*Brink*, 2013; *Bruns et al.*, 2016]. However, also a combination of burial and uplift together with an intrusion may explain the gravity high [*Bilgili et al.*, 2009]. *Bruns and Littke* [2015] mentioned that moderate heat flow conditions prevailed during burial in the Lower Saxony Basin, which generally agrees to our model setup.

Smaller scale organic maturity highs such as Roxfoerde-Velpke Asse granitic intrusions or the Lippstadt dome at the northern end of the Rhenish Massif are assumed to be of late Variscan age [*Koch et al.*, 1997]. In contrast to the Bramsche Massif, 9 m granitic intrusion were confirmed for the Velpke-Asse borehole with a presumably early Permian age [*Brink et al.*, 1992].

The organic maturity highs Uchte and Vlotho up to Sollingen, which were pointed to Mesozoic volcanic intrusions [*Koch et al.*, 1997], can be questioned similarly to the Bramsche Massif. This area is in line with the Harz mountains up to the Netherlands part of the Lower Saxony Basin, which underwent uplift due to the Late Cretaceous inversion [*de Jager*, 2003], especially when considering the offset of the Egge-Fault. Perhaps, there is a relation between this line in form of a northwest to southeast direction, since interpolated isoreflectance lines show a similar direction [*Drozdzewski et al.*, 2009].

The assumed Erkelenz intrusion [*Erren and Bredewout*, 1991] might also be questioned similar to the Bramsche Massif. Northwest to southeast oriented isoreflectance lines [*Erren and Bredewout*, 1991] point to a non-circular spatial influence, such as a potential Late Cretaceous deep burial and subsequent exhumation event. In addition, *Erren and Bredewout* [1991] argues against his own interpretation that either felsic or mafic intrusions lack either geophysical or geological explanation. In Figure 22, the Erkelenz intrusion is not well observable, because Zechstein formation and Upper Rotliegend are not preserved, yet the surrounding area shows similar, but weaker tendencies.

4.6 Exhumation in the frame of the Variscan deformation front

The Variscan deformation front has been traced by several authors based on geophysical surveys and field observations [*Von Hartmann*, 2003; *Drozdzewski et al.*, 2009; *Mazur et al.*, 2010; *Dulce and Lewis,* 2011; *Krzywiec et al.*, 2016]. However, important differences in the interpretation of the location of the Variscan deformation front exist.

Drozdzewski et al. [2009] proposes a deformation front that closely follows the current southern limit of the Northeast German Basin up to the wide area between the Pompeckj Block and Harz Mountains. *Dulce and Lewis* [2011] argue with seismic tracks that Carboniferous beneath the Lower Saxony Basin is also folded. Therefore, they locate the Variscan deformation front much more north between the Lower Saxony Basin and Pompeckj Block. This is in agreement with *Von Hartmann* [2003], who limits the northern possible extent with interpretation of three-dimensional seismic data to the southern boundary of the Pompeckj Block.

In contrast, *Drozdzewski et al.* [2009] state that the lack of seismic surveys and boreholes data denies giving exact details. They argue that local structures of the Lower Saxony Basin show wrench style tectonics and reactivation in the Late Cretaceous. This idea is accompanied by the hypothesis that the Osning fault is a transfer zone between the Harz Mountains and the Rhenish Mountains due to their different shortening and later reactivation in the Late Cretaceous [*Drozdzewski et al.*, 2009].

Our organic maturity misfit results (Figure 22) show high differences between modeled and measured vitrinite reflectance in the Variscan deformation front to the south of the proposed line by *Drozdzewski et al.* [2009], which suggest exhumation of deeper buried rocks.

However, large differences in organic maturity are for the Lower Saxony Basin and the Pompeckj Block at least partially explainable by Late Cretaceous exhumation and overprinted at least in the Lower Saxony most or all signals of pre-Permian exhumation.

Yet, this argument seems not feasible, when going further northeast to the most east proposed location of the Variscan deformation front by *Dulce and Lewis* [2011]. In contrast to the proposed position by *Drozdzewski et al.* [2009], the organic maturity is not likely explainable by todays burial depth (Figure 1), especially when considering the isoreflectance maps of pre-Permian and base of Zechstein by *Koch et al.* [1997]. Strong influence of tectonic events such as Late Cretaceous inversion [*Kley and Voigt*, 2008] are yet to be shown for this area. Intrusions as heat sources are due to extent and form of the organic maturity misfit unlikely (Figure 22). However, large extrusive volcanic rocks exist [*Heeremans et al.*, 2004].

Likewise, the positon of the Variscan deformation in Poland is challenged [*Krzywiec et al.*, 2016]. The proposed location of *Pozaryski et al.* [1992] for the Variscan deformation front somewhere in the Polish Lowland in large distance to the East European Craton agrees more to *Drozdzewski et al.* [2009]. But due to the interpretation of new seismic data, *Krzywiec et al.* [2016] argue that the Variscan deformation front is terminated by the East European Craton. They assume a complex system of pre-Permian thin-skinned compressional deformation up to the Lublin Basin and Radom-Krasnik Block.

However, the tectonic models of the Teisseyre-Tornquist-Zone are also confronted, because for example the exact positon of the East European Craton is extensively discussed [*Mazur et al.*, 2015, 2016; *Dziewinska and Tarkowski*, 2016]. Nonetheless, these discussions suggest that the Variscan deformation front terminates within the Polish Trough.

This basin is filled with large Mesozoic sediments, for which *Resak et al.* [2008] and we have argued, that Mesozoic burial reaches levels of organic maturity, which overprint possible Variscan deformation front and subsequent exhumation related organic maturity. Though, *Krzywiec et al.* [2016] does not argue against the classical view that the Variscan deformation front is leaving the Polish Trough westwards into the Northeast German Basin [*Pozaryski et al.*, 1992].

Anyhow, two observations might be drawn by interpreting Figure 22, which agree to *Krzywiec et al.* [2016]. Firstly, large differences between modeled and measured organic maturity point to Variscan deformation and subsequent exhumation in the southwest of the Polish Trough. Secondly, the Variscan deformation front may have extended to the northeastern boundary of the Lublin Basin. Regardless, this result should be considered with great care, because the area of the Lublin Basin is small and interpolation errors likely. However, the uncertainty could be decreased by using local borehole data, due to its small area.

Even more challenging seems the location of the Variscan deformation front between the Polish Trough and the most east location *Dulce and Lewis* [2011] propose. There are seismic survey data available such as DEKORP or EGT, but the quality is not enough to distinct foreland from orogeny [*Franke*, 1995]. Also, only very few wells exist, which penetrate pre-Permian [*Resak et al.*, 2008]. This however complicates interpolation, so the certainty of the organic maturity data of the SPBA [*Doornenbal and Stevenson*, 2010] is low.

However, it is not likely that the Variscan deformation front terminates as south as *Drozdzewski et al.* [2009] assumes, because in this area large differences are observable between modeled Upper Rotliegend and measured pre-Permian (Figure 23). Instead, 20 to 40 km north is a jump with more than 1.5 % vitrinite reflectance difference between measured and modeled data, which can be traced back to the Polish Trough (Figure 23). This jump does more or less agree to the interpretation by *Pozaryski et al.* [1992], since the jump enters the Polish Trough 20 to 30 km southwards. Additionally, the Brandenburg-Wolsztyn-Pogorzela high is situated there and at least the highs are considered to be deformed by the Variscan deformation [*Kiersnowski et al.*, 2010].

On the other side to *Dulce and Lewis* [2011], the jump in vitrinite reflectance even suggest a more northeastern location of the Variscan deformation front, since deviations of 2.2 to 2.4 % vitrinite reflectance are calculated there. Additionally, we believe that relatively good data exist for the south of the Glueckstadt Graben and since our model agrees to the local organic maturity model by *Rodon and Littke* [2005], it is perhaps not wrong to discuss even a Variscan deformation front located north than *Dulce and Lewis* [2011] suggested. From there on, the Variscan deformation front would enter the Pompeckj Block and later the Lower Saxony Basin.

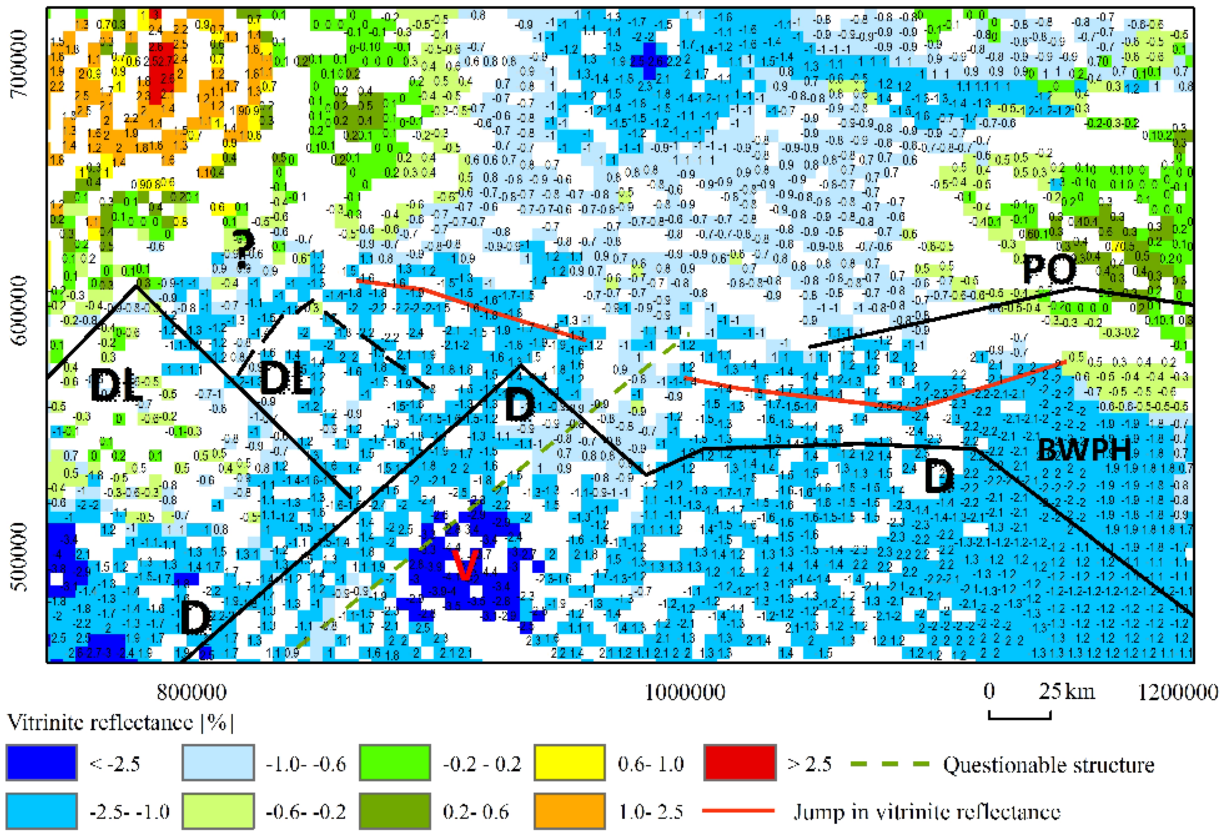

Figure 23. Variscan deformation fronts shown in organic maturity misfit map (Figure 22). Variscan deformation fronts adapted from *Dulce and Lewis* [2011] (DL), *Drozdzewski et al.* [2009] (D) and *Pozaryski et al.* [1992] (PO). Brandenburg-Wolsztyn-Pogorzela high (BWPH), Velpke-Asse intrusion (V). Question mark (?) shows potential northern location of the Variscan deformation front.

Besides, one may argue for two other observations. Firstly, a southwest to northeast trending questionable structure is indicated by vitrinite reflectance misfit, which perhaps show a Variscan structure.

Secondly, the not well constrained connection between *Dulce and Lewis* [2011] and *Pozaryski et al.* [1992] perhaps forms a structure, which opens in northeastern direction. This might indicate extensional structures potentially related to the Lower Rotliegend volcanism. The presumably early Permian Velpke-Asse intrusion might be connected to the extension [*Brink et al.*, 1992].

However, these hypotheses have to be treated carefully, since the certainty and availability of published data is especially low for the Northeast German Basin. For future research, confirmation by published borehole data of the pre-Permian is necessary.

5 Sadler effect

The Sadler effect states that with increasing time span, observed sedimentation and accumulation rates decrease in a negative power law relationship [*Sadler*, 1981; *Schumer and Jerolmack*, 2009].

The nature of the relationship between preserved sedimentation, time span and geological variables like tectonic settings are still debated. Here we investigate whether the Sadler effect is observable in the Mesozoic and Cenozoic sedimentary fill of the Central European Basin System as a whole and in individual sub-basins. We explore whether the Sadler effect is describable by power law or similar heavy-tail equations and whether the equation type and parameter have any relations with geological settings of the various basins in the Central European Basin System.

5.1 Theory of the Sadler effect

Tipper [2016] questions whether the Sadler effect is distributed as a power law or not, but does not find a definitive answer. Nevertheless, he clarifies the Sadler effect by defining commonly used terms. *Tipper* [2016] defines sedimentation systems as complexes of inter-related processes including transport, sedimentation, omission and erosion. *McKee et al.* [1983] highlights the importance to distinguish between sedimentation and accumulation as the latter describes only the net sum of deposited material minus erosion.

The difference between sedimentation and accumulation rate is not observable, because sediments may only have been partly preserved. The proportion of preserved sediments is described by the preservation rate, which is influenced by the inter-related processes of a sedimentation system. Conclusively, the necessary properties for estimating accumulation rates are the time span and the thickness of the section, while for estimating the sedimentation rate, the preservation rate is additionally required [*Sadler*, 1999].

Tipper [2016] argues that a sedimentation rate is calculated by stochastic variables, which is also the case for accumulation rates. Hence, the variable accumulation rate changes its values by chance variation of the variables thickness and time span of a section. This chance variation is dependent on the result of random processes, uncertain definition of the variables itself, measurement imprecision or sampling effects [*Tipper*, 2016].

Any changes in the preservation rate are therefore dependent on its chance variation, which are influenced by geologic variables. As a consequence, to show if the Sadler effect may be useful for describing erosion, the Sadler effect must fulfill a functional relationship, but must also inhibit changes in geologic variables.

5.2 Method

We reconstruct accumulation rates from measured thickness, which is in this study calculated from thickness data [*Doornenbal and Stevenson*, 2010] and surface elevation dataset ETOPO1 [*Amante and Eakings*, 2009] for the area of the Central European Basin System (CEBS) [*Ziegler*, 1990; *Littke et al.*, 2008]. The equation to calculate accumulation rates of a basin is based on measured thickness and their correlated ages:

$$\mathrm{r} = \sum_{\mathrm{i=1}}^{\mathrm{i=n}} \frac{\left(\frac{th}{t}\right)}{\mathrm{n}}, \tag{3}$$

where $\left(\frac{th}{t}\right), \mathrm{i} = 1 \ldots \mathrm{n}$ are accumulation rates from measured thickness th and time span t. The variable r refers to the arithmetic mean of the accumulation rate for an in each case specified basin. As r is an arithmetic mean, r is shown as bin value in the study.

We fit a power law equation to the observed accumulation rates, following:

$$\mathrm{p(r)} = \mathrm{C} \cdot \mathrm{r}^{-\mathrm{a}}, \tag{4}$$

where accumulation rate r is drawn from accumulation rates of a basin, a is the scaling parameter or exponent and value C is a constant [*Clauset et al.*, 2009].

We investigated if the accumulation rates follow a power law relation, following *Clauset et al.* [2009], including the two-sample Kolmogorow-Smirnov test [*Smirnov*, 1948] as implemented in the python script Powerlaw [*Alstott et al.*, 2014]. Additionally, we transformed the variables time span and accumulation rate into log units, which are used for establishing a linear regression by least squares estimation:

$$l = a + bx, \tag{5}$$

$$b = \frac{\sum_{i=n}^{n}(x_i - \bar{x})\,(y_i - \bar{y})}{\sum_{i=n}^{n}(x_i - \bar{x})^2}, \tag{6}$$

$$a = \bar{y} - b\bar{x}, \tag{7}$$

where l is the linear regression line, $\bar{y}$ and $\bar{x}$ are arithmetic averages of x_i and y_i, as well as $\mathrm{i} = 1 \ldots \mathrm{n}$ are measurements [*Hartung et al.*, 2009]. x is based on t and y is based on r (Equation 3).

5.3 Result

To describe the nature of the Sadler effect relationship, we present accumulation rates r in a frequency plot for the total area of the CEBS. This plot states that the frequency of r is lower, the higher r is.

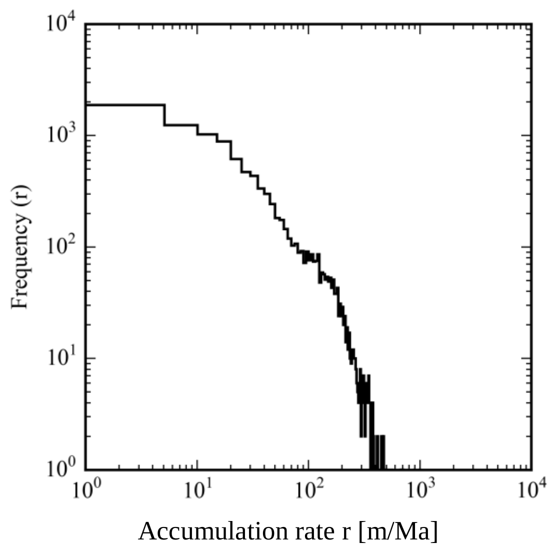

Figure 24. Frequency plot of accumulation rate of all lithologies of the CEBS used in this study (r). The distribution is non-strict linear.

The use of the two-sample Kolmogorow-Smirnov [*Smirnov*, 1948; *Clauset et al.*, 2009; *Alstott et al.*, 2014] test did not produce unambiguously fits for ideal (truncated) power laws, (stretched) exponential or lognormal distribution functions.

Nevertheless, when calculating average r for each lithology of the total CEBS, a strict power law equation is derived by excluding Quaternary accumulation rates (see discussion) using least square estimation [*Bretscher*, 2004] in the form of equation 4 (Figure 25):

$$\mathrm{f(r)} = 621.12 \cdot \mathrm{r}^{-1.157}. \tag{8}$$

The data is transformed into log units, resulting in a linear relationship. This statistical transformation is chosen because it increases the observability of low r. Power laws ought to be analyzed in log-log plots and statistical measures are derivable [*Clauset et al.*, 2009]. Applying equation 5, we derived the linear regression:

$$l = -0.78r + 2.26. \quad (9)$$

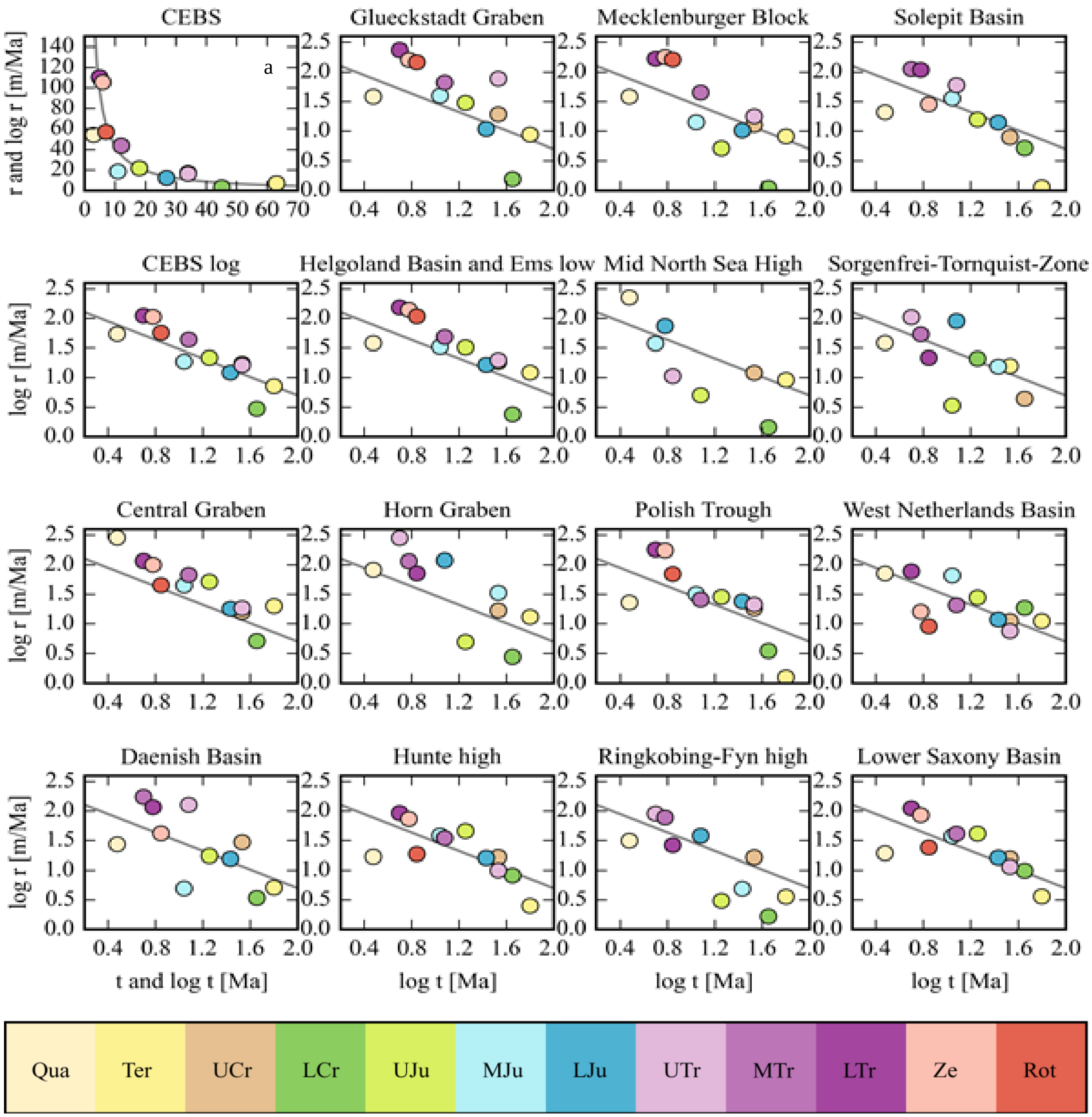

Figure 25. Accumulation rates versus duration for sub-basins in the Central European Basin System. All plots are in log units, except plot a. The plot a shows a heavy-tail distribution of the arithmetic average accumulation compared to time span of each lithology for the CEBS. This might be a power law near distribution. The other plots show the CEBS and several sub-basins. The grey lines follow their respective equations 8 and 9. This plot shows that the Sadler effect is not only present in the total CEBS, but also in sub-basins. Nevertheless, some values differ from

the trend of the Sadler effect largely. For abbreviations, see next Figure.

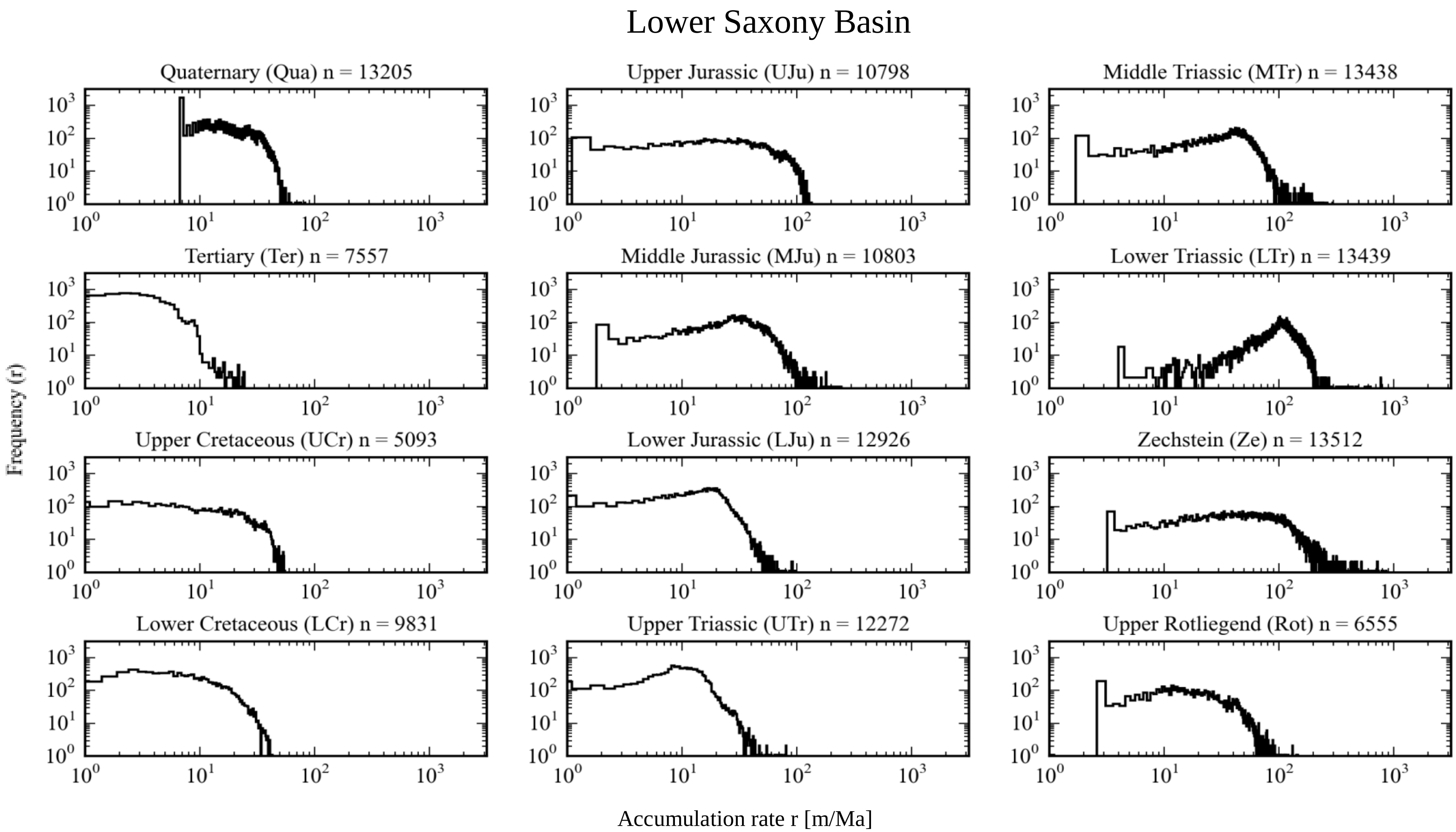

Figure 26. Frequency plots of accumulation rate (r) of formations of the Lower Saxony Basin. Most plots show the general heavy-tail trend of Figure 24, except for Zechstein up to Middle Jurassic. In this time span, higher accumulation rates are more preserved than lower accumulation rates.

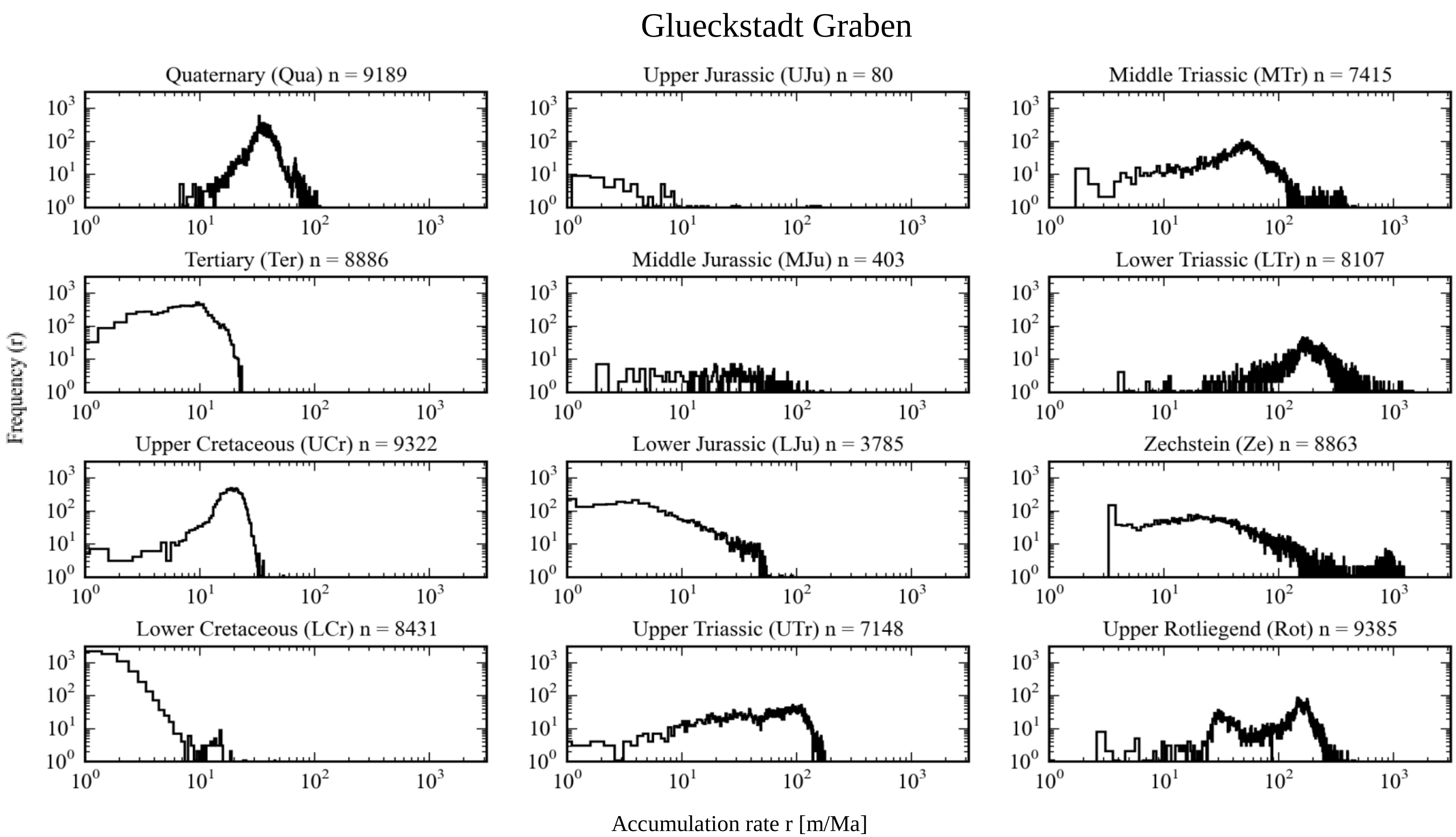

Figure 27. Frequency plots of accumulation rate (r) of formations of the Glueckstadt Graben. Only Tertiary, Lower Jurassic and maybe Zechstein show the general heavy-tail trend of Figure 24.

5.4 Discussion

5.4.1 Sadler effect in relation to accumulation rates

As remarked by *Clauset et al.* [2009] and agreeing to the call into question by *Tipper* [2016], the Sadler effect like many power laws might not be truly distributed as a power law. A linear distribution of the regression of the assumed power law in a log unit plot is a necessary condition for accepting a functional relationship between two stochastic variables as a power law relationship [*Clauset et al.*, 2009], which is not the case for the whole distribution (Figure 24).

However, because of taking the average of accumulation rates for each formation of the CEBS, instead of taking the average of accumulation rates for every single value for every lithology, a power law relationship is established (Figure 25) and chosen for deriving the power law (Equation 8).

In opposite, we cannot exclude other heavy-tail distributions with statistical tests. Yet, heavy-tailed distributions are better statistical analyzable than power law distributions [*Clauset et al.*, 2009] and therefore provide more potential for future research. Conclusively, in the further discussion we call the distributions heavy-tail distribution.

A single sedimentation rate depends on truncated normal distributions, as the duration of a time span for calculating the sedimentation rate is never completely preserved [*Tipper*, 2016]. As accumulation is a product of sedimentation processes, we assume that an accumulation rate also follows a truncated normal distribution Adding or subtracting of underlying truncated normal distributed data would result in a lognormal distribution of accumulation rates. However, the lognormal distribution was the least likely fitting distribution in this study for the SPBA dataset [*Smirnov*, 1948; *Clauset et al.*, 2009].

This agrees to *Tipper* [2016], as he concludes that the heavy-tail distribution is only secondarily a result due to depositional processes, which vary and produce truncated normal distributions. Primarily, the heavy-tail distribution is due to the last-in-first-out principle [*Tipper*, 2016]. This principle describes processes, in which only the top of a stack is influenced by adding or subtracting deposition processes [*Tipper*, 2016].

Anyway, Figure 24, 26, 27 and the Figures in the appendix show that there are definitely returning functional relationships between time span and accumulation rate produced by repeating forms (curves) in different plots, which point to systematically behavior of accumulation rates. We assume that these forms are the reflection of the Sadler effect influenced by different deposition processes of deposition regimes.

5.4.2 Mechanism between deposition regimes and accumulation rates

As it seems, there are two main forms of functional relationship observable in Figures 26 and 27. One repeating form is distributed as a heavy-tail distribution (similar to Figure 24). The second repeating form shows a maximum in the distribution and is maybe describable as leptokurtic. Additionally, there are examples where both main forms are mixed.

The heavy-tail distributed form agrees to the Sadler effect [*Sadler*, 1981] and thus, follows potentially the commonest deposition regime in the CEBS and is perhaps explained by the last-in-first-out principle [*Tipper*, 2016].

However, the position of the slope of a heavy-tail distribution to the abscissa hypothetically points to the shape of a basin, because high accumulation rates are situated mostly within a deposition center, while low accumulation rates should occur near the basin margin.

When the top of a basin is eroded, the proportion of eroded material between deposition center and margin is different, insofar the preserved proportion of material in deposition centers is more. This leads to a leptokurtic distribution.

The leptokurtic distribution could additionally be produced by increased accumulation rates, when the proportion of low accumulation rates in a basin decrease, which may be the case for closed basins, where the deposition system changed form last-in-first-out to all-in. This implicates that the whole form moves to higher accumulation rates along the abscissa.

In opposite, leptokurtic distributions produced by erosion events should agree to the position of the steepest slope of the heavy-tailed distribution. Erosion event could also decrease the count of measurements, when basin flanks are completely eroded.

To the contrary, phases of omission alike conditions should however not decrease the count of measurements, but produce low accumulation rates with the abscissa position of the heavy-tailed distribution.

When one would normalize the count of measurements between basins, maybe more exact statements about the geologic variables could be made considering especially the position on the abscissa.

5.4.3 Local examples

For the Lower Saxony Basin, the frequencies of accumulation rates (Figure 26) follow mostly the heavy-tail relationship of Figure 24. *Senglaub et al.* [2005] summarizes that between late Permian to Late Jurassic a continuous sedimentation took place, which begun with the Zechstein formation and ended with strong subsidence in the Late Jurassic. This time span is potentially observable in Figure 26, since high accumulation rates are more frequent than low accumulation rates, but generally follow the heavy-tail relationship or even leptokurtic distribution produced by erosion.

Further, the inversion during the Late Cretaceous in the Lower Saxony Basin [*Betz et al.*, 1987] is likely represented by the frequency plot as the number of measurements (n) is low and may be explained by erosion. However, no leptokurtic distribution is found, which deny the aforementioned relationships or simply state that the time of deposition after the inversion was long enough to overprint the leptokurtic distribution.

For the Glueckstadt Graben, the frequency of accumulation rates (Figure 27) follows only during Early Jurassic and Zechstein formation the heavy-tail relationship of Figure 24. An erosional leptokurtic distribution is observed for the Late Jurassic and Late Cretaceous.

The aforementioned relationships are not able to explain the distribution of the Lower Cretaceous in the Glueckstadt Graben on the first view, because it seems to follow low accumulation rates, which may point to omission, yet the maximum abscissa position disagrees. However, a very small leptokurtic peak potentially points to a not described combination of geologic events, such as local salt tectonic leading to few measurements with high accumulation rates.

Maystrenko et al. [2005] state in their first conclusion that there are indications for an increasing subsidence in the Buntsandstein formation up until the Keuper formation, which is possibly observable in Figure 27.

The Upper Rotliegend of the Glueckstadt Graben shows two peaks, where one is at the position of the heavy-tailed distribution, while the second is moved along larger abscissa values.

In both basins, the Zechstein formation shows increased accumulation rates and possibly a closed basin situation.

Further, we found no certain explanation for the gap in low accumulation rates in Upper Rotliegend up to Middle Triassic, and Middle Jurassic and Quaternary (Figures 26, 27). But likely, low thicknesses of these formations are not included into the SPBA dataset.

The Quaternary offset may also be explainable by the influence of the Pleistocene on accumulation rates, where sediments are transported fast into the North Sea. Alternatively, the missing low accumulation rates are explainable by the thickness calculation algorithm and possibly an artifact. These various reasons lead to the removal of the Quaternary for establishing the equation 8.

After applying possible mechanism on two sub-basins of the CEBS, which influence the accumulation rates distribution in a frequency plot, we confirm that the Sadler effect is a statistical effect and *Tippers* [2016] hypotheses, that the Sadler effect is a distribution produced by different processes, seems likely. In addition, this statistical effect is indeed interpretable in regard of analyzing geologic processes, such as deposition regimes in relation to accumulation rates. Promising for future research is the fairly easy use as far as a thickness dataset exists To extract geologic information, a classification of the accumulation rate distributions in a frequency plot is necessary, but also normalization of measurements may be advisable.

6 Conclusion

This study shows that it is possible to reproduce present-day subsurface temperature data in a large scale approach by using heat flow data, estimated surface temperatures and calibrating one lithological properties dataset. With the reproduced present-day subsurface temperature data, a burial and thermal history model of the Central European Basin System from late Permian to present-day was constructed.

The plausibility is constrained by comparing modeled to measured organic maturity. To be in line with measured geological history, discussing areas with challenging salt tectonics, high amounts of exhumation or volcanism is necessary.

With analyzing misfits of organic maturity, the unconformity between top Carboniferous and late Permian is investigated from a different point of view than usual, e.g. seismic or stratigraphic research. In the Northeast German Basin, Lower Rotliegend intrusive volcanic rocks are responsible for increased organic maturity. In addition, the location of the Variscan deformation front is traced with differences in modeled and measured organic maturity between late Permian and pre-Permian.

The creation of the burial and thermal history model for the Central European Basin System was successful and these map compilations can be a valuable asset when comparing sub-basins or local geologic history. For example, relations between irregularities in organic maturities of the Erkelenz intrusion and the Bramsche Massif are drawn.

Moreover, the heavy-tail functional relationship of the Sadler effect is observed for the Central European Basin System and a general equation was derived. However, the certainty and conclusive adjustments of the equation are subject to further research. Further, links between accumulation rates and geologic variables such as deposition regimes are perceived in frequency plots and appear to be promising study objects for the future as they might be classifiable.

Finally, the thermal and burial history model and the Sadler effect show that time and space are important factors for exploring new geological relations between sub-basins.

7 Acknowledgment

Firstly, I would like to say the greatest thanks to Prof. Dr. Jonas Kley, who always had an open door whenever I ran into difficulties regarding complex geological matter.

Further, I cannot express enough thanks to Dr. Elco Luijendijk for his continued support and encouragements. He proposed the topic of the Master's thesis and steered me into the right direction, whenever he thought I needed it.

But I want to thank both my supervisors also for their lectures, in which I improved my knowledge about structural geology and modeling.

I would like to acknowledge GFZ — Section 6.1 Basin Modeling for handing the fundamental heat flow dataset out, which is an important part for building a reasonable burial and thermal history model.

The completion of my study could not have been accomplished without the support of my friends. I would like to thank Christian Berner, Dennis Grabow, Stefan Strube, Jan Schoenig and Philipp Ulbrich for discussions and helpful ideas for the Master's thesis.

At last but not least, I would like to thank my family for their friendship, appreciation and support.

8 References

Allen, P. A., and J. R. Allen (2005), *Basin Analysis: Principles and Applications*, Second Edi., Blackwell Publishing.

Alstott, J., E. Bullmore, and D. Plenz (2014), Powerlaw: A python package for analysis of heavy-tailed distributions, *PLoS One*, *9*(1), doi:10.1371/journal.pone.0085777.

Amante, C., and B. W. Eakings (2009), ETOPO1 1 Arc-Minute Global Relief Model: Procedures, Data Sources and Analysis, NOAA Technical Memorandum NESDIS NGDC-24, *Natl. Geophys. Data Cent.*, doi:10.7289/V5C8276M.

Athy, L. F. (1930), Density, porosity, and compaction of sedimentary rocks, *Am. Assoc. Pet. Geol. Bull.*, *14*(1), 1–24.

Bahr, D. B., E. W. H. Hutton, J. P. M. Syvitski, and L. F. Pratson (2001), Exponential approximations to compacted sediment porosity profiles, *Comput. Geosci.*, *27*(6), 691–700, doi:10.1016/S0098-3004(00)00140-0.

Bertani, R. (2016), Geothermal power generation in the world 2010–2014 update report, *Geothermics*, *60*, 31–43, doi:10.1016/j.geothermics.2015.11.003.

Betz, D., F. Fohrer, G. Greiner, E. Plein, and G. Plein (1987), Evolution of the Lower Saxony Basin, *Tectonophysics*, *137*, 127–170, doi:10.1016/0040-1951(87)90319-2.

Bilgili, F., H. J. Goetze, R. Pašteka, S. Schmidt, and R. Hackney (2009), Intrusion versus inversion - A 3D density model of the southern rim of the Northwest German Basin, *Int. J. Earth Sci.*, *98*(3), 571–583, doi:10.1007/s00531-007-0267-y.

Bond, G. C., and M. A. Kominz (1984), Construction of tectonic subsidence curves for the early Paleozoic miogeocline, southern Canadian Rocky Mountains: implications for subsidence mechanisms, age of breakup, and crustal thinning (Canada), *Geol. Soc. Am. Bull.*, *95*(2), 155–173.

Botor, D., B. Papiernik, T. Maekowski, B. Reicher, P. Kosakowski, G. Machowski, and W. Górecki (2013), Gas generation in Carboniferous source rocks of the Variscan foreland basin: Implications for a charge history of Rotliegend deposits with natural gases, *Ann. Soc. Geol. Pol.*, *83*, 353–383.

Bretscher, O. (2004), *Linear Algebra With Applications*, 3rd ed., Prentice Hall, Upper Saddle River.

Brink, H.-J. (2013), Die Intrusion von Bramsche – ein Irrtum im invertierten Niedersächsischen Becken?, *Zeitschrift der Dtsch. Gesellschaft für Geowissenschaften*, *164*(1), 33–48, doi:10.1127/1860-1804/2013/0011.

Brink, H. J., H. Duerschner, and H. Trappe (1992), Some aspects of the late and post-Variscan development of the Northwestern German Basin, *Tectonophysics*, *207*, 65–95.

Bruns, B., and R. Littke (2015), Lithological dependency and anisotropy of vitrinite reflectance in high rank sedimentary rocks of the Ibbenbueren area, NW-Germany: Implications for the tectonic and thermal evolution of the Lower Saxony Basin, *Int. J. Coal Geol.*, *137*, 124135, doi:10.1016/j.coal.2014.11.007.

Bruns, B., R. Littke, M. Gasparik, J. D. van Wees, and S. Nelskamp (2016), Thermal evolution and shale gas potential estimation of the Wealden and Posidonia Shale in NW-Germany and the Netherlands: A 3D basin modelling study, *Basin Res.*, *28*(1), 2–33.

Cacace, M., M. Scheck-Wenderoth, V. Noack, Y. Cherubini, and R. Schellschmidt (2013), Modelling the Surface Heat Flow Distribution in the Area of Brandenburg (Northern Germany), *Energy Procedia*, *40*, 545–553, doi:10.1016/j.egypro.2013.08.063.

Clark, D. N. (1986), The Distribution of Porosity in Zechstein Carbonates, in *Habitat of Palaeozoic Gas in N. W. Europe*, edited by J. Brooks, J. C. Goff, and B. Van Hoorn, pp. 121–149, Geological Society Special Publication.

Clauser, C., and E. Huenges (2013), Thermal Conductivity of Rocks and Minerals, *Rock Phys. Phase Relations*, 105–126, doi:10.1029/RF003p0105.

Clauset, A., C. R. Shalizi, and M. E. J. Newman (2009), Power-Law Distributions in empirical data, *SIAM Rev. 51*, 661–703, doi:10.1137/070710111.

Courant, R. (1943), Variational methods for the solution of problems of equilibrium and vibrations., *Bull. Amer. Math. Soc.*, *49*(1), 1–23.

Doornenbal, H., and A. Stevenson (2010), *Petroleum Geological Atlas of the Southern Permian Basin Area*, EAGE.

Drozdzewski, G., S. Henscheid, P. Hoth, D. Juch, R. Littke, A. Vieth, and V. Wrede (2009), The pre-Permian of NW-Germany – structure and coalification map, *Zeitschrift der Dtsch. Gesellschaft für Geowissenschaften*, *160*(2), 159–172, doi:10.1127/1860-1804/2009/0160-0159.

Dulce, B. J., and D. S. Lewis (2011), Variscan Deformation of Carboniferous Strata North of the Lower Saxony Basin, NW Germany – 3D Interpretation of Intra-Carboniferous Reflections, *OIL GAS Eur. Mag.*, *4*, 184–186.

Dziewinska, L., and R. Tarkowski (2016), Geophysical study of deep basement structure of NW Poland using effective reflection coefficients, *Comptes Rendus Geosci.*, *348*(8), 587–597, doi:10.1016/j.crte.2016.06.003.

Erren, H., and J. W. Bredewout (1991), Model calculations on intrusive cooling and related coalification of the Peel-Erkelenz Coalfield (The Netherlands and Germany), *Geol. en Mijnb.*, *70*, 243–252.

Foerster, A. (2001), Analysis of borehole temperature data in the Northeast German Basin: continuous logs versus bottom-hole temperatures, *Pet. Geosci.*, *7*(3), 241–254, doi:10.1144/petgeo.7.3.241.

Franke, D. (1995), The North Variscan Foreland, in *Pre-Permian Geology of Central and Western Europe*, edited by R. D. Dallmeyer, W. Franke, and K. Weber, pp. 555–566, Springer.

Fuchs, S., and N. Balling (2016a), Improving the temperature predictions of subsurface thermal models by using high-quality input data. Part 1: Uncertainty analysis of the thermal-conductivity parameterization, *Geothermics*, *64*, 42–54, doi:10.1016/j.geothermics.2016.04.010.

Fuchs, S., and N. Balling (2016b), Improving the temperature predictions of subsurface thermal models by using high-quality input data. Part 2: A case study from the Danish-German border region, *Geothermics*, *64*, 1–14, doi:10.1016/j.geothermics.2016.04.004.

Fuchs, S., N. Balling, and A. Foerster (2015), Calculation of thermal conductivity, thermal diffusivity and specific heat capacity of sedimentary rocks using petrophysical well logs, *Geophys. J. Int.*, *203*(3), 1977–2000, doi:10.1093/gji/ggv403.

Geißler, M., C. Breitkreuz, and H. Kiersnowski (2008), Late paleozoic volcanism in the central part of the Southern Permian Basin (NE Germany, W Poland): Facies distribution and volcano-topographic hiati, *Int. J. Earth Sci.*, *97*(5), 973–989, doi:10.1007/s00531-007-0288-6.

Gerling, P., M. C. Celuk, F. Kockel, A. Lokhorst, G. K. Lott, and R. A. Nicholson (1999), 'NW European Gas Atlas'–new implications for the Carboniferous gas plays in the western part of the Southern Permian Basin, *Geol. Soc. London, Pet. Geol. Conf. Ser.*, *5*, 799–808.

Goesl, S., and R. Govers (2000), Shallow mantle temperatures under Europe from P and S wave tomography, *J. Geophys. Res.*, *105*, 153–169.

Green, P. F. (1992), Thermal history reconstruction in two onshore Netherlands wells using apatite fission track analysis and vitrinite reflectance, *Geotrack Int.*

Von Hartmann, H. (2003), Deformation of the Carboniferous on the Oldenburg High and the Location of the Variscan Front in Northwest Germany, *Netherlands J. Geosci.*, *82*(2), 169–176.

Hartung, J., B. Elpelt, and K.-H. Kloesener (2009), *Statistik: Lehr- und Handbuch der angewandten Statistik*, 15. überar., Oldenburg Wissenschaftsverlag GmbH.

Heeremans, M., J. I. Faleide, and B. T. Larsen (2004), Late Carboniferous - Permian of NW Europe: an introduction to a new regional map, *Geol. Soc. London Spec. Publ.*, *223*, 75–88.

Helsen, S., and V. Langenaeker (1999), Burial history and coalification modelling of Westphalian strata in the eastern Campine Basin (northern Belgium), *Geol. Surv. Belgium Prof. Pap.*, *289*, 23.

Hossein, S. Z. et al. (2006), Lithospheric structure of the Tornquist Zone resolved by nonlinear P and S teleseismic tomography along the TOR array, *Tectonophysics*, *416*(1–2), 133–149, doi:10.1016/j.tecto.2005.11.019.

Integrated Geochemical Interpretation Ltd. (1996), Geochemical elements of the petroleum system in the greater Waalwijk field area, south Netherlands, Technical report,

de Jager, J. (2003), Inverted basins in the Netherlands, similarities and differences, *Geol. en Mijnbouw/Netherlands J. Geosci.*, *82*(4), 355–366.

Japsen, P., P. F. Green, L. H. Nielsen, E. S. Rasmussen, and T. Bidstrup (2007), Mesozoic-Cenozoic exhumation events in the eastern North Sea Basin: A multi-disciplinary study based on palaeothermal, palaeoburial, stratigraphic and seismic data, *Basin Res.*, *19*(4), 451–490, doi:10.1111/j.1365-2117.2007.00329.x.

Jaupart, C., J. C. Mareschal, and L. Iarotsky (2016), Radiogenic heat production in the continental crust, *Lithos*, *262*, 398–427, doi:10.1016/j.lithos.2016.07.017.

Jensen, P. K. (1983), Calculations on the Thermal Conditions Around a Salt Diapir, *Geophys. Prospect.*, *31*(3), 481–489, doi:10.1111/j.1365-2478.1983.tb01064.x.

Kerschke, D. I., and H. M. Schulz (2013), The shale gas potential of Tournaisian, Visean, and Namurian black shales in North Germany: Baseline parameters in a geological context, *Environ. Earth Sci.*, *70*(8), 3817–3837, doi:10.1007/s12665-013-2745-9.

Kiersnowski, H., T. M. Peryt, A. Buniak, and Z. Mikołajewski (2010), From the intra-desert ridges to the marine carbonate island chain: middle to late Permian (Upper Rotliegend-Lower Zechstein) of the Wolsztyn-Pogorzela high, west Poland, *Geol. J.*, *45*(2–3), 319–335, doi:10.1002/gj.1189.

Kley, J., and T. Voigt (2008), Late Cretaceous intraplate thrusting in central Europe: Effect of Africa-Iberia-Europe convergence, not Alpine collision, *Geology*, *36*(11), 839–842, doi:10.1130/G24930A.1.

Koch, J., F. Kockel, and P. Krull (1997), Coalification at the Zechstein and the pre-Permian surface in northern Germany, *Thirty years Appl. Hydrocarb. Res. Fed. Inst. Geosci. Nat. Resour.*, *103*, 33–42.

Kroner, U., and R. L. Romer (2013), Two plates - Many subduction zones: The Variscan orogeny reconsidered, *Gondwana Res.*, *24*(1), 298–329, doi:10.1016/j.gr.2013.03.001.

Krzywiec, P., S. Mazur, Ł. Gągała, M. Kufrasa, M. Lewandowski, M. Malinowski, and V. Buffenmyer (2016), Late Carboniferous thin-skinned compressional deformation above the SW edge of the East European Craton as revealed by reflection seismic and potential fields data – correlations with the Variscides and the Appalachians, in *Linkages and Feedbacks in Orogenic Processes*, edited by R. Law, R. Thigpen, H. Stowell, and M. A, Geological Society of America Publishing House.

Limberger, J. (2014), Geoelec data supplement, *Utr. Univ.*, doi:http://dx.doi.org/10.4121/uuid:91fe7c44-9798-491e-a807-5ca40b9f2093.

Littke, R., U. Bayer, D. Gajewski, and S. Nelskamp (2008), *Dynamics of Complex Intracontinental Basins: The Central European Basin System*.

Luijendijk, E., R. T. Van Balen, M. Ter Voorde, and P. A. M. Andriessen (2011a), Reconstructing the Late Cretaceous inversion of the Roer Valley Graben (southern Netherlands) using a new model that integrates burial and provenance history with fission track thermochronology, *J. Geophys. Res. Solid Earth*, *116*(6), doi:10.1029/2010JB008071.

Luijendijk, E., M. Ter Voorde, R. Van Balen, H. Verweij, and E. Simmelink (2011b), Thermal state of the Roer Valley Graben, part of the European Cenozoic Rift System, *Basin Res.*, *23*(1), 65–82, doi:10.1111/j.1365-2117.2010.00466.x.

Majorowicz, J., and S. Wybraniec (2011), New terrestrial heat flow map of Europe after regional paleoclimatic correction application, *Int. J. Earth Sci.*, *100*(4), 881–887, doi:10.1007/s00531-010-0526-1.

Maystrenko, Y., U. Bayer, and M. Scheck-Wenderoth (2005), The Glueckstadt Graben, a sedimentary record between the North and Baltic Sea in north Central Europe, *Tectonophysics*, *397*, 113–126, doi:10.1016/j.tecto.2004.10.004.

Maystrenko, Y. P., and M. Scheck-Wenderoth (2013), 3D lithosphere-scale density model of the Central European Basin System and adjacent areas, *Tectonophysics*, *601*, 53–77, doi:10.1016/j.tecto.2013.04.023.

Maystrenko, Y. P., U. Bayer, and M. Scheck-Wenderoth (2013), Salt as a 3D element in structural modeling - Example from the central european basin system, *Tectonophysics*, *591*, 62–82, doi:10.1016/j.tecto.2012.06.030.

Mazur, S., P. Aleksandrowski, K. Turniak, L. Krzemiński, K. Mastalerz, A. Górecka-Nowak, L. Kurowski, P. Krzywiec, A. Zelaźniewicz, and M. C. Fanning (2010), Uplift and late orogenic deformation of the Central European Variscan belt as revealed by sediment provenance and structural record in the Carboniferous foreland basin of western Poland, *Int. J. Earth Sci.*, *99*(1), 47–64, doi:10.1007/s00531-008-0367-3.

Mazur, S., M. Mikolajczak, P. Krzywiec, M. Malinowski, V. Buffenmyer, and M. Lewandowski (2015), Is the Teisseyre-Tornquist Zone an ancient plate boundary of Baltica?, *Tectonics*, *34*(12), 2465–2477, doi:10.1002/2015TC003934.

Mazur, S., M. Mikolajczak, P. Krzywiec, M. Malinowski, M. Lewandowski, and V. Buffenmyer (2016), Pomeranian Caledonides, NW Poland – A collisional suture or thin-skinned fold-and-thrust belt?, *Tectonophysics*, *692*, 29–43, doi:10.1016/j.tecto.2016.06.017.

McKee, B. A., C. A. Nittrouer, and D. J. Demaster (1983), Concepts of sediment deposition and accumulation applied to the continental shelf near the mouth of the Yangtze River (China)., *Geology*, *11*, 631–633, doi:10.1130/0091-7613(1983)11<631:COSDAA>2.0.CO;2.

Meier, T., R. Soomro, L. Viereck, S. Lebedev, H. J. Behrmann, C. Weidle, L. Cristiano, and R. Hanemann (2016), Mesozoic and Cenozoic evolution of the Central European lithosphere, *Tectonophysics*, doi:10.1016/j.tecto.2016.09.016.

Menning, M., D. Weyer, I. Wendt, G. Drozdzewksi, and U. Hambach (2005), Eine numerische Zeitskala für das Pennsylvanium in Mitteleuropa, *Cour. Senckenb.*, *254*, 181.

Narkiewicz, M., M. Resak, R. Littke, and L. Marynowski (2010), New constraints on the middle Palaeozoic to Cenozoic burial and thermal history of the Holy Cross Mts. (central Poland): Results from numerical modelling, *Geol. Acta*, *8*(2), 189–205, doi:10.1344/105.000001529.

Nielsen, S. B., O. R. Clausen, and E. Mcgregor (2015), basin%Ro: A vitrinite reflectance model derived from basin and laboratory data, *Basin Res.*, doi:10.1111/bre.12160.

NLOG (2016), Maturity at Top Carboniferous, Available from: http://nlog.nl/en/maturity (Accessed 20 January 2016)

Noack, V., M. Scheck-Wenderoth, and M. Cacace (2012), Sensitivity of 3D thermal models to the choice of boundary conditions and thermal properties: A case study for the area of Brandenburg (NE German Basin), *Environ. Earth Sci.*, *67*(6), 1695–1711, doi:10.1007/s12665-012-1614-2.

Petmecky, S., L. Meier, H. Reiser, and R. Littke (1999), High thermal maturity in the Lower Saxony Basin: intrusion or deep burial?, *Tectonophysics*, *304*(4), 317–344, doi:10.1016/S0040-1951(99)00030-X.

Pharaoh, T. C. (1999), Palaeozoic terranes and their lithospheric boundaries within the Trans-European Suture Zone (TESZ): A review, *Tectonophysics*, *314*(1–3), 17–41, doi:10.1016/S0040-1951(99)00235-8.

Pozaryski, W., A. Grocholski, H. Tomcyzk, P. Karnkowski, and W. Moryc (1992), The tectonic map of Poland in the Variscan epoch, *Przegl. Geo.*, *40*(11), 643–651.

Regenspurg, S., E. Feldbusch, B. Norden, and M. Tichomirowa (2016), Fluid-rock interactions in a geothermal Rotliegend/Permo-Carboniferous reservoir (North German Basin), *Appl. Geochemistry*, *69*, 12–27, doi:10.1016/j.apgeochem.2016.03.010.

Resak, M., M. Narkiewicz, and R. Littke (2008), New basin modelling results from the Polish part of the Central European Basin system: Implications for the Late Cretaceous - Early paleogene structural inversion, *Int. J. Earth Sci.*, *97*(5), 955–972, doi:10.1007/s00531-007-0246-3.

Revil, A., and M. Cathles (1999), Permeability of shaly sands, *Water Resour.*, *35*(3), 651–662.

Rodon, S., and R. Littke (2005), Thermal maturity in the Central European Basin system (Schleswig-Holstein area): Results of 1D basin modelling and new maturity maps, *Int. J. Earth Sci.*, *94*(5–6), 815–833, doi:10.1007/s00531-005-0006-1.

Sachse, V. F., and R. F. Littke (2016), Burial, temperature and maturation history of the Ringkøbing-Fyn High, Denmark, *Zeitschrift der Dtsch. Gesellschaft für Geowissenschaften*, *167*(2), 249–268, doi:10.1127/zdgg/2016/0052.

Sadler, P. M. (1981), Sediment Accumulation Rates and the Completeness of Stratigraphic Sections, *J. Geol.*, *89*(5), 569–584, doi:10.1086/628623.

Sadler, P. M. (1999), The Influence of Hiatuses on Sediment Accumulation Rates, *GeoResearch Forum*, *5*, 15–40.

Scheck-Wenderoth, M., and J. Lamarche (2005), Crustal memory and basin evolution in the Central European Basin System - New insights from a 3D structural model, *Tectonophysics*, *397*(1–2 SPEC. ISS.), 143–165, doi:10.1016/j.tecto.2004.10.007.

Scheck-Wenderoth, M., and Y. P. Maystrenko (2013), Deep Control on Shallow Heat in Sedimentary Basins, *Energy Procedia*, *40*, 266–275, doi:10.1016/j.egypro.2013.08.031.

Scheck-Wenderoth, M., M. Cacace, Y. P. Maystrenko, Y. Cherubini, V. Noack, B. Kaiser, R. Onno, J. Sippel, and L. Björn (2014), Models of heat transport in the Central European Basin System: Effective mechanisms at different scales, *Mar. Pet. Geol.*, *55*, 315–331, doi:10.1016/j.marpetgeo.2014.03.009.

Schoen, J. H. (2015), *Physical Properties of Rocks: Fundamentals and Principles of Petrophysics*, Vol. 65., Elsevier.

Schumer, R., and D. J. Jerolmack (2009), Real and apparent changes in sediment deposition rates through time, *J. Geophys. Res. Solid Earth*, *114*(3), 1–12, doi:10.1029/2009JF001266.

Senglaub, Y., M. R. Brix, A. C. Adriasola, and R. Littke (2005), New information on the thermal history of the southwestern Lower Saxony Basin, northern Germany, based on fission track analysis, *Int. J. Earth Sci.*, *94*(5–6), 876–896, doi:10.1007/s00531-005-0008-z.

Smirnov, N. (1948), Table for Estimating the Goodness of Fit of Empirical Distributions, *Ann. Math. Stat.*, *19*(2), 279–281, doi:10.1214/aoms/1177730256.

Stampfli, G. M., J. F. von Raumer, and G. D. Borel (2002), Paleozoic evolution of pre-Variscan terranes: from Gondwana to the Variscan collision, *Geol. Soc. Am. Spec. Pap.*, *364*, 263–280, doi:10.1130/0-8137-2364-7.263.

Steckler, M. S., and A. B. Watts (1978), Subsidence of the Atlantic-type continental margin off New York, *Earth Planet. Sci. Lett.*, *41*(1), 1–13, doi:10.1016/0012-821X(78)90036-5.

Sweeney, J. J., and A. K. Burnham (1990), Evaluation of a simple model of vitrinite reflectance based on chemical kinetics, *Am. Assoc. Pet. Geol. Bull.*, *74*(10), 1559–1570.

Teichmueller, M., R. Teichmueller, and H. Bartenstein (1979), Inkohlung und Erdgas in Nordwestdeutschland. Eine Inkohlungskarte der Oberfläche des Oberkarbons, *Geol. Landesamt Nord.*, (27).

Thybo, H. (2000), Crustal structure and tectonic evolution of the Tornquist Fan region as revealed by geophysical methods, *Bull. Geol. Soc. Denmark*, *46*, 145–160.

Timmerman, M. J. (2004), Timing, geodynamic setting and character of Permo-Carboniferous magmatism in the foreland of the Variscan Orogen, NW Europe, *Geol. Soc. London, Spec. Publ.*, *223*, 41–74, doi:10.1144/GSL.SP.2004.223.01.03.

Tipper, J. C. (2016), Measured rates of sedimentation: What exactly are we estimating, and why?, *Sediment. Geol.*, *339*, 151–171, doi:10.1016/j.sedgeo.2016.04.003.

Van Wees, J. D., R. A. Stephenson, P. A. Ziegler, U. Bayer, T. McCann, R. Dadlez, R. Gaupp, M. Narkiewicz, F. Bitzer, and M. Scheck (2000), On the origin of the Southern Permian Basin, Central Europe, *Mar. Pet. Geol.*, *17*(1), 43–59, doi:10.1016/S0264-8172(99)00052-5.

Wilson, M., E.-R. Neumann, G. R. Davies, M. J. Timmerman, M. Heeremans, and B. T. Larsen (2004), Permo-Carboniferous magmatism and rifting in Europe: introduction, *Permo-Carboniferous Magmat. Rift. Eur.*, *223*, 1–10, doi:10.1144/GSL.SP.2004.223.01.01.

Yegorova, T., U. Bayer, H. Thybo, Y. Maystrenko, M. Scheck-Wenderoth, and S. B. Lyngsie (2007), Gravity signals from the lithosphere in the Central European Basin System, *Tectonophysics*, *429*(1–2), 133–163, doi:10.1016/j.tecto.2006.10.002.

Zhang, J. (2013), Effective stress, porosity, velocity and abnormal pore pressure prediction accounting for compaction disequilibrium and unloading, *Mar. Pet. Geol.*, *45*, 2–11, doi:10.1016/j.marpetgeo.2013.04.007.

Zhuo, Q. G., F. W. Meng, M. J. Zhao, Y. Li, X. S. Lu, and P. Ni (2016), The salt chimney effect: delay of thermal evolution of deep hydrocarbon source rocks due to high thermal conductivity of evaporites, *Geofluids*, *16*(3), 440–451, doi:10.1111/gfl.12162.

Ziegler, P. A. (1990), *Geological atlas of western and central Europe.*, Geological Society of London.

9 Declaration

Ich versichere hiermit, dass ich die vorliegende Arbeit ohne fremde Hilfe selbstständig verfasst und nur die von mir angegebenen Quellen und Hilfsmittel verwendet habe. Wörtlich oder sinngemäß aus anderen Werken entnommene Stellen habe ich unter Angabe der Quellen kenntlich gemacht.

Die Richtlinien zur Sicherung der guten wissenschaftlichen Praxis an der Universität Göttingen wurden von mir beachtet. Eine gegebenenfalls eingereichte digitale Version stimmt mit der schriftlichen Fassung überein. Mir ist bewusst, dass bei Verstoß gegen diese Grundsätze die Prüfung mit nicht bestanden bewertet wird.

Göttingen, den Tom Kaltofen